Introduction to Superconducting Quantum Circuits

2

Michael Stern

Abstract

Standard textbooks on quantum mechanics typically illustrate the theory using examples from the microscopic world, such as atoms, electrons or molecules. At this scale, quantum effects are striking and easily noticeable. At the macroscopic level, quantum mechanics seems however often counter-intuitive. Features like state superposition and entanglement lead to well-known logical paradoxes, challenging our understanding of what we call 'reality'. Controlling quantum features in a macroscopic physical object could open the way for building a new generation of quantum machines with tremendous computational power. Superconducting electrical circuits are an example of such a macroscopic quantum system. As of today, the cutting-edge level of control exhibited by these circuits has led them to be considered as one of the foremost technologies for physically implementing quantum computers. Moreover, it is possible to make hybrid systems in which the quantum variables of an electrical circuit are coupled to various microscopic degrees of freedom, thereby demonstrating that these circuits constitute a general interface to the quantum world. The purpose of this chapter is to provide an introduction to superconducting quantum circuits, elucidating how such systems can exhibit quantum behavior and how they can be controlled to serve as a building block of quantum processors.

M. Stern (✉)
Quantum Nanoelectronics Laboratory, Department of Physics, Bar Ilan University, Ramat Gan, Israel
e-mail: michael.stern@biu.ac.il

R. Aguado et al. (eds.), *New Trends and Platforms for Quantum Technologies*,
Lecture Notes in Physics 1025, https://doi.org/10.1007/978-3-031-55657-9_2

2.1 Quantization of an Electrical Circuit

2.1.1 The Lumped-Element Circuit Model

We will first begin with some reminders concerning classical electrical circuits in the radio-frequency or microwave domain ($f \sim 1$ MHz–100 GHz). For simplicity, we consider a circuit formed by a planar network of electrical dipoles. This lumped element description is valid when the physical size of the circuit is much smaller than the wavelength λ of the signal.

2.1.1.1 Constitutive Relations

At any instant t, the classical state of a dipole can be fully determined by knowing a single dynamical variable. One can measure either $V(t)$ which represents the voltage drop across the dipole or $I(t)$ the current flowing through it. These two dynamical variables are connected to each other by a constitutive relation. This constitutive relation may be linear (e.g. Ohm law) or non linear and characterizes the dipole element. It is often more convenient to describe the state of the dipole by the charge and flux variables, namely $Q(t)$ and $\Phi(t)$ defined as

$$\boxed{\begin{aligned}\dot{Q}(t) &= I(t)\\ \dot{\Phi}(t) &= V(t)\end{aligned}} \tag{2.1}$$

Capacitive elements such as capacitors ($V = Q/C$) have constitutive relations where the voltage drop depends only on charge. Their energy *only* depends on charge:

$$E = \int V(t)I(t)\,dt = \int V(Q)\dot{Q}(t)\,dt = \int V(Q)\,dQ \tag{2.2}$$

Inductive elements have constitutive relations where the current depends only on flux. This function can be linear ($I = \Phi/L$) or non-linear (e.g. $I = I_0 \sin(\Phi/\varphi_0)$). Their energy *only* depends on flux:

$$E = \int I(t)V(t)\,dt = \int I(\Phi)\dot{\Phi}(t)\,dt = \int I(\Phi)\,d\Phi \tag{2.3}$$

2.1.1.2 Defining the Spanning Tree of a Circuit

To solve the circuit, one needs first to define a set of independent variables taking into account these constitutive relations. According to graph theory, a planar network of dipoles with similar constitutive relations (i.e. only resistors or only capacitors) can be reduced to a single equivalent dipole. One can therefore find systematically a set of independent variables by the so-called *node method.* This method consists of:

1. finding first all the nodes of the circuit which connect at least two elements with *distinct* constitutive relations, and associating to each of them an electrical potential.
2. Defining a set of independent fluxes $(\Phi_1, \Phi_2, \ldots, \Phi_n)$ by drawing a *spanning tree* which access every node without forming a loop, preferably passing through inductors only.

To write the equation of motion of the circuit, we use Kirchhoff's node law, which expresses charge conservation, and which states that the sum of currents flowing into a node is equal to the sum of currents flowing out of that node. The hypothesis of charge conservation is well verified in usual metals below their plasma frequency, which is usually in the deep UV range, far above microwave frequencies.

2.1.1.3 A Simple Example

To illustrate our point, let us consider the example shown in Fig. 2.1. The points A and B are nodes of the circuit and are characterized by electrical potentials V_A and V_B . Point C connects three purely resistive elements and thus the elements connected to this point can be reduced to a single equivalent dipole of resistance $R_{eq} = R_1 + \frac{R_2 R_3}{R_2 + R3}$. The spanning tree connecting node A and B defines here a single independent flux variable Φ, the flux threading the inductance L.

We write the equation of motion of the circuit by writing Kirchhoff law at node A and using the constitutive relations of each element:

$$I(t) = i_L(t) + i_C(t) + i_R(t) = \frac{\Phi}{L} + C\ddot{\Phi} + \frac{\dot{\Phi}}{R_{eq}} \tag{2.4}$$

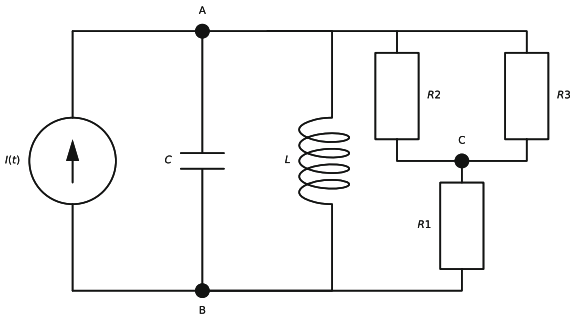

Fig. 2.1 Simple example of a lumped element circuit. A current source $I(t)$ is connected to a network of dipole elements. Points A and B are nodes of the circuit. Point C connects three purely resistive elements and thus can be reduced to a single resistive dipole. The flux threading the inductance $\dot{\Phi}(t) = V_A(t) - V_B(t)$ can be chosen as the dynamical variable of the system

where $\dot{\Phi}(t) = V_A(t) - V_B(t)$, $i_L(t) = \frac{\Phi}{L}$ is the current flowing in the inductor branch, $i_C(t) = C\ddot{\Phi}$ the current flowing in the capacitor branch, and $i_R(t) = \frac{\dot{\Phi}}{R_{eq}}$ the current flowing in the resistive branch.

2.1.2 Quantization of a Lumped Element Circuit

To ensure the quantum mechanical behavior of a circuit, the first requirement is the *absence of dissipation*. Specifically, all metallic components must be constructed from materials that exhibit zero resistance at the circuit's frequency and operating temperature. Zero resistance is obtained by fabricating the circuit out of a metal, which becomes superconducting at low temperatures. Superconductivity arises from the pairing and condensation of electrons with opposite spins into a special ground state [1]. This ground state possesses an excitation gap, 2Δ, which is the energy required to disrupt one of the electron pairs and create an excited state. It is this excitation gap that enables current to flow through a superconductor without dissipation. Additionally, this gap reduces the number of effective degrees of freedom in the circuit, allowing the construction of circuits that behave quantum mechanically, despite being composed of approximately 10^{12} atoms.

In addition, the remaining degrees of freedom of the circuit must be cooled to temperatures where the typical energy of thermal fluctuations is much less that the energy associated with the transition frequency of the circuit. For instance, if the circuit operates at 5 GHz, the required operating temperature should be approximately 20 mK (keeping in mind that 5 GHz corresponds to about 0.25 K). Achieving such temperatures can be accomplished by cooling the circuit using a dilution refrigerator. However, it is equally crucial to cool the wires connected to the circuit's control and readout ports, which can bring a substantive amount of heat to the system. This last point requires meticulous electromagnetic filtering.

2.1.2.1 Definition of the Conjugate Variables

For an arbitrary circuit composed of non dissipative elements, one obtains the equation of motion by first identifying the independent variables as stated in Sect. 1.1 and writing the Lagrangian of the system

$$\mathcal{L} = K(\dot{\Phi}_1, \dot{\Phi}_2 \ldots, \dot{\Phi}_n) - U(\Phi_1, \Phi_2, \ldots, \Phi_n) \tag{2.5}$$

where K is the capacitive energy and U the inductive energy of the circuit. The conjugate momenta of our system are given by

$$Q_i \equiv \frac{\partial \mathcal{L}}{\partial \dot{\Phi}_i} \tag{2.6}$$

Finally, one obtains the Hamiltonian of the system by writing $\mathcal{H} = \sum \dot{\Phi}_i Q_i - \mathcal{L}$. From this point, the equation of motion can be directly obtained.

$$\dot{\Phi}_i = \frac{\partial \mathcal{H}}{\partial Q_i}$$
$$\dot{Q}_i = -\frac{\partial \mathcal{H}}{\partial \Phi_i}$$

The principle of correspondence of Dirac stipulates that one can quantize the system by introducing the operators $\hat{\Phi}_i$ and $\hat{Q}_i$ which obey commutation relations

$$\boxed{\left[\hat{\Phi}_i, \hat{Q}_i\right] = i\hbar} \tag{2.7}$$

2.1.2.2 From the Capacitance Matrix to the Hamiltonian of the Circuit

Let us now consider the example shown in Fig. 2.2. The points A, B and C are nodes of the circuit and are characterized by electrical potentials V_A, V_B and V_C. We define a spanning tree by choosing the flux Φ_1 and Φ_2 shown in the figure and connecting these three nodes.

The inductive energy U of the system is simply given by

$$U = \frac{\Phi_1^2}{2L_1} + \frac{\Phi_2^2}{2L_2} \tag{2.8}$$

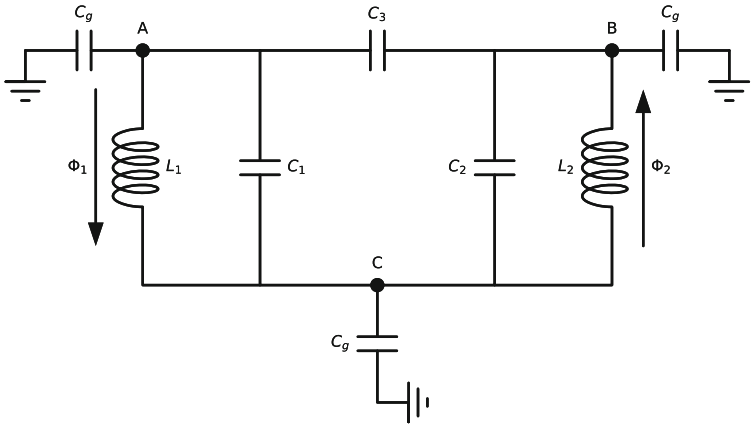

Fig. 2.2 Quantization of two coupled resonators. Each bare resonator is composed of an inductor of inductance $L_{1,2}$ in parallel with a capacitor of capacitance $C_{1,2}$. They are coupled directly by the capacitor C_3 and indirectly via their coupling to the ground. The points A, B and C are nodes of the circuit. The fluxes Φ_1 and Φ_2 define a spanning tree connecting all the three nodes

The capacitive energy K of the system is given by

$$K = \frac{1}{2}C_1(V_A - V_C)^2 + \frac{1}{2}C_2(V_B - V_C)^2 + \frac{1}{2}C_3(V_A - V_B)^2 + \frac{1}{2}C_g V_A^2 + \frac{1}{2}C_g V_B^2 + \frac{1}{2}C_g V_C^2$$

It is possible to write the capacitive energy as $K = \frac{1}{2}\mathbf{V}^T\mathbf{C}\mathbf{V}$ where $\mathbf{V^T} = (V_A, V_B, V_C)$ and $\mathbf{C}$ is a 3×3 matrix which we will refer in the following as the *capacitance matrix*. In our case,

$$\mathbf{C} = \begin{pmatrix} C_1 + C_3 + C_g & -C_3 & -C_1 \\ -C_3 & C_2 + C_3 + C_g & -C_2 \\ -C_1 & -C_2 & C_1 + C_2 + C_g \end{pmatrix} \tag{2.9}$$

Using the definitions $\dot{\Phi}_1 = V_C - V_A$, $\dot{\Phi}_2 = V_B - V_C$ and Millman theorem [2] for the ground voltage $V_g = V_A + V_B + V_C \equiv 0$, we have

$$\begin{cases} V_A &= -\frac{2}{3}\dot{\Phi}_1 - \frac{1}{3}\dot{\Phi}_2 \\ V_B &= +\frac{1}{3}\dot{\Phi}_1 + \frac{2}{3}\dot{\Phi}_2 \\ V_C &= +\frac{1}{3}\dot{\Phi}_1 - \frac{1}{3}\dot{\Phi}_2 \end{cases}$$

Thus, one can define a passage matrix $\mathbf{P}$ that expresses $\mathbf{V}$ as a function of $\dot{\mathbf{\Phi}} = (\dot{\Phi}_1, \dot{\Phi}_2)$, i.e. $\mathbf{V} = \mathbf{P}\dot{\mathbf{\Phi}}$. It is therefore possible to write the Lagrangian $\mathcal{L}$ as

$$\mathcal{L} = \frac{1}{2}\dot{\mathbf{\Phi}}^T\widetilde{\boldsymbol{C}}\dot{\mathbf{\Phi}} - \frac{1}{2}\mathbf{\Phi}^T L^{-1}\mathbf{\Phi} \tag{2.10}$$

where $\boldsymbol{L}^{-1} = \begin{pmatrix} 1/L_1 & 0 \\ 0 & 1/L_2 \end{pmatrix}$ and $\widetilde{\boldsymbol{C}} = \mathbf{P}^T\mathbf{C}\mathbf{P}$. The conjugate momenta of our system are given by $\boldsymbol{Q} = (Q_1, Q_2) \equiv \widetilde{\boldsymbol{C}}\dot{\mathbf{\Phi}}$ and the Hamiltonian is thus given by

$$\boxed{\mathcal{H} = \frac{1}{2}\boldsymbol{Q}^T\widetilde{\boldsymbol{C}}^{-1}\boldsymbol{Q} + \frac{1}{2}\mathbf{\Phi}^T\boldsymbol{L}^{-1}\mathbf{\Phi}} \tag{2.11}$$

2.1.2.3 Coupling Between Two Resonators

The Hamiltonian herein above can be greatly simplified if one assumes that $C_3, C_g \ll C_1, C_2$. In this case, one can write easily $\widetilde{\boldsymbol{C}}^{-1}$ as

$$\widetilde{\boldsymbol{C}}^{-1} \simeq \frac{1}{C_1 C_2}\begin{pmatrix} C_2 + C_3 + \frac{2}{3}C_g & C_3 + \frac{1}{3}C_g \\ C_3 + \frac{1}{3}C_g & C_1 + C_3 + \frac{2}{3}C_g \end{pmatrix} \tag{2.12}$$

By grouping the quadratic terms of each independent variable with its conjugate, it is straightforward to show that one can write $\mathcal{H}$ as the sum of two harmonic oscillators with a coupling term V

$$\mathcal{H} = \mathcal{H}_1 + \mathcal{H}_2 + V \tag{2.13}$$

where

$$\mathcal{H}_1 = \hbar\omega_1(a_1^+ a_1 + \frac{1}{2}) \tag{2.14}$$

$$\mathcal{H}_2 = \hbar\omega_2(a_2^+ a_2 + \frac{1}{2}) \tag{2.15}$$

$$\omega_i^2 = \frac{1}{L_i}\left[\tilde{\boldsymbol{C}}^{-1}\right]_{ii} \tag{2.16}$$

and

$$V = \frac{C_3 + \frac{1}{3}C_g}{C_1 C_2} Q_1 Q_2 = \hbar\eta\sqrt{\omega_1\omega_2}(a_1 - a_1^+)(a_2^+ - a_2) \tag{2.17}$$

with $\eta \simeq \frac{C_3+\frac{1}{3}C_g}{\sqrt{C_1 C_2}}$ and where $a_{1,2}$ and $a_{1,2}^+$ are the creation and annihilation operators of each harmonic oscillator. Even without a direct coupling capacitance $C_3 \equiv 0$, an indirect coupling between the resonators is established via their coupling to the ground. This point illustrates a general difficulty in the design of superconducting quantum circuits. Indeed, isolating circuits is difficult due to to their large coupling with the surrounding environment.

2.1.3 Transmission Lines

Contrary to lumped element circuits, the physical dimensions of transmission lines are comparable to the wavelength λ of the signal [3]. Thus, a transmission line is a distributed-parameter network, where voltage and currents can vary in magnitude and phase over its length.

2.1.3.1 Definition of the Propagation Wave Amplitudes

A transmission line can be modeled by a series of discrete lumped elements as shown in Fig. 2.3. The inductance per unit cell u is L_u and the capacitance to the ground per unit cell is C_u.

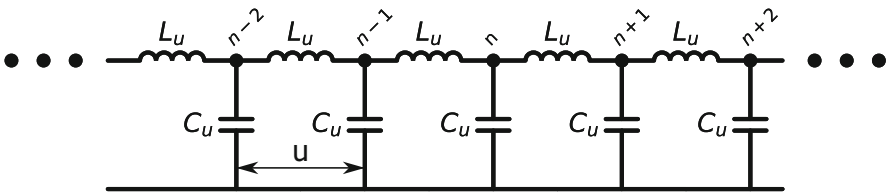

Fig. 2.3 Circuit model of a transmission line. The transmission line is modelled by a series of discrete lumped elements. The unit cell length is u. The inductance per unit cell is L_u and the capacitance per unit cell is C_u

We write the equations for the voltage and currents in the transmission line using the constitutive relations of the dipole elements and Kirchhoff charge conservation

$$\begin{aligned} V_{n+1} - V_n &= -L_u \partial_t I_{n\to n+1} \\ -C_u \partial_t V_n &= I_{n\to n+1} - I_{n-1\to n} \end{aligned}$$

Going to the continuum limit where $L_u/u \to \mathscr{L}$ and $C_u/u \to \mathscr{C}$, we get

$$\begin{aligned} \partial_x V(x,t) &= -\mathscr{L}\partial_t I(x,t) \\ -\mathscr{C}\partial_t V(x,t) &= \partial_x I(x,t) \end{aligned}$$

To solve these coupled differential equations, we define the propagation wave amplitudes $A^{\rightarrow}$ and $A^{\leftarrow}$ by

$$\boxed{\begin{aligned} A^{\rightarrow} &= \frac{1}{2}\left(V/\sqrt{Z_0} + I\sqrt{Z_0}\right) \\ A^{\leftarrow} &= \frac{1}{2}\left(V/\sqrt{Z_0} - I\sqrt{Z_0}\right) \end{aligned}} \tag{2.18}$$

where $Z_0 = \sqrt{\mathscr{L}/\mathscr{C}}$ and obtain two decoupled first order differential equations

$$\begin{aligned} \partial_t A^{\rightarrow} + c\partial_x A^{\rightarrow} &= 0 \\ \partial_t A^{\leftarrow} - c\partial_x A^{\leftarrow} &= 0 \end{aligned}$$

where $c = 1/\sqrt{\mathscr{L}\mathscr{C}}$ is the propagation velocity in the transmission line. The solutions are of the form $A^{\rightarrow}(x,t) = \mathscr{A}_{out}(x - ct)$ and $A^{\leftarrow}(x,t) = \mathscr{A}_{in}(x + ct)$ where $\mathscr{A}_{in}$ and $\mathscr{A}_{out}$ are arbitrary functions of their arguments. For an infinite transmission line, $\mathscr{A}_{in}$ and $\mathscr{A}_{out}$ are completely independent. Interestingly, the

instantaneous power $\mathcal{P}(x,t)$ is directly related to the square of the propagation wave amplitudes

$$\boxed{\mathcal{P}(x,t) = I(x,t) \times V(x,t) = \mathscr{A}_{out}^2 - \mathscr{A}_{in}^2} \tag{2.19}$$

2.1.3.2 Fourier Components of the Propagation Wave Amplitudes

Since the equations are linear, it is possible to look at individual Fourier components[1] of $A^{\rightarrow/\leftarrow}(x,t)$ at any given point in space x.

$$A^{\rightarrow/\leftarrow}(x,t) = \sum_k A_k^{\rightarrow/\leftarrow}(x)\, e^{-i\omega_k t} + \text{c.c.} \tag{2.20}$$

In the following sections, we will consider monochromatic waves only, thus dropping the sum and index k systematically. We write

$$A^{\rightarrow/\leftarrow}(x,t) = A^{\rightarrow/\leftarrow}(x)\, e^{-i\omega t} + \text{c.c.} \tag{2.21}$$

Assuming $\mathscr{A}_{in} = 0$ and using Eq. (2.19), we get

$$\begin{aligned}\mathcal{P}(x,t) = \mathscr{A}_{out}^2 &= \left(A^{\rightarrow}(x)\, e^{-i\omega t} + \text{c.c.}\right)^2 \\ &= 2\left|A^{\rightarrow}(x)\right|^2 + \left((A^{\rightarrow}(x))^2\, e^{-2i\omega t} + \text{c.c.}\right)\end{aligned}$$

Thus, the modulus of $|A^{\rightarrow}(x)|^2$ is proportional to the average power $\langle P(x)\rangle = \lim_{T\to\infty} \frac{1}{T}\int_0^T \mathcal{P}(x,t)\, dt$

$$\boxed{\langle P(x)\rangle = 2\left|A^{\rightarrow}(x)\right|^2} \tag{2.22}$$

2.1.3.3 Semi-Infinite Transmission Line

When a semi-infinite transmission line is terminated at $x = 0$ by some system S the two solutions $\mathscr{A}_{in}$ and $\mathscr{A}_{out}$ are related by boundary conditions imposed by the system.

$$V(x=0,t) = \sqrt{Z_0}(\mathscr{A}_{out}(t) + \mathscr{A}_{in}(t))$$

$$I(x=0,t) = \frac{1}{\sqrt{Z_0}}(\mathscr{A}_{out}(t) - \mathscr{A}_{in}(t))$$

[1] We adopt the quantum convention for wave propagation (i.e. $e^{i(kx-\omega t)}$), which differs by a sign from the one found typically in the microwave textbooks (i.e. $e^{i(\omega t-kx)}$).

If the system S is an open circuit, $I(x=0,t)=0$ and thus $\mathscr{A}_{out}(t)=\mathscr{A}_{in}(t)$. If the system S is short circuit, $V(x=0,t)=0$ and thus $\mathscr{A}_{out}(t)=-\mathscr{A}_{in}(t)$. The outgoing waves are simply the result of the incoming wave reflecting from the open/short circuit termination.

In the absence of an incoming wave $\mathscr{A}_{in}(t)=0$, we have $V(x=0,t)=Z_0 I(x=0,t)$ indicating that the transmission line acts as a resistance which instead of dissipating energy by heat carries the energy away from the system as propagating waves.

2.1.4 Quantization of a Transmission Line

Hamiltonian dynamics is inherently reversible and thus dissipationless. Irreversibility however arises when the number of degrees of freedom grows to infinity. In the quantum framework, it was shown that a dissipative impedance can be rigourously taken into account by using the so-called Caldeira Leggett decomposition [4], which consists of modelling any dissipator by an infinite collection of LC resonators. Another way to model dissipation for non-dissipative elements in electrical circuits is to consider an ideal semi-infinite transmission line [5]. As shown in the classical approach herein above, any signal sent down the line will never come back and thus there is a loss of information and entropy creation.

2.1.4.1 Hamiltonian of a Transmission Line

In order to illustrate this point, let us consider a transmission line of length Λ formed by a series of N cells as shown in Fig. 2.4. We assume periodic boundary conditions such that $V_N=V_0$. For each cell of size u, the inductive (potential) energy can be written as $U_n=\frac{\Phi_n^2}{2L_u}$ and the capacitive (kinetic) energy as $K_n=\frac{1}{2}C_u V_n^2$.

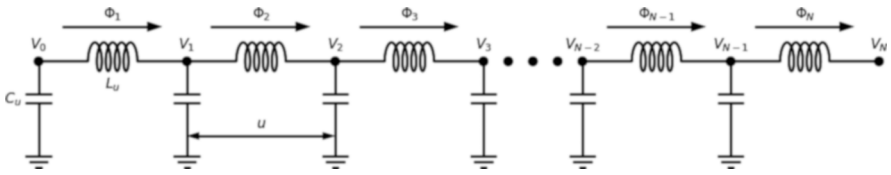

Fig. 2.4 Discrete model for quantization of a transmission line. We denote as V_n the voltage of node n and Φ_n the flux through the inductor between node $n-1$ and n. The cell unit length is u , the inductance per unit cell is L_u and capacitance per unit cell is C_u. We assume periodic boundary conditions such that $V_N=V_0$

Using $\dot{\Phi}_{n+1} = V_{n+1} - V_n$, one can write

$$V_i = \sum_{j=1}^{i} \dot{\Phi}_j + V_0$$

By summing all the equations together and using Millman theorem [2] $\left(\sum_{n=0}^{N-1} V_n = 0\right)$, we get $V_0 = -\sum_{n=1}^{N-1} V_n = -\left((N-1)\dot{\Phi}_1 + (N-2)\dot{\Phi}_2 + \ldots + \dot{\Phi}_{N-1} + (N-1)V_0\right)$. These equations define a passage matrix $\mathbf{P}$ that expresses the vector $\mathbf{V} = (V_0, \ldots . V_{N-1})$ as a function of $\dot{\mathbf{\Phi}} = (\dot{\Phi}_1, \ldots, \dot{\Phi}_N)$, i.e. $\mathbf{V} = \mathbf{P}\dot{\mathbf{\Phi}}$.

It is thus possible to write the Lagrangian of the system $\mathcal{L}$ as

$$\mathcal{L} = \frac{1}{2} C_u \dot{\Phi}^T \mathbf{P}^T \mathbf{P} \dot{\Phi} - \frac{1}{2L_u} \Phi^T \Phi \tag{2.23}$$

The conjugate momenta of our system are given by $\boldsymbol{Q} = (Q_1, \ldots, Q_N) \equiv \frac{\partial \mathcal{L}}{\partial \dot{\mathbf{\Phi}}}$ and the Hamiltonian is thus given by

$$\mathcal{H} = \frac{1}{2C_u} \boldsymbol{Q}^T \begin{pmatrix} 2 & -1 & 0 & \ldots & -1 \\ -1 & 2 & -1 & \ddots & \vdots \\ 0 & -1 & \ddots & \ddots & 0 \\ \vdots & \ddots & \ddots & 2 & -1 \\ -1 & \cdots & 0 & -1 & 2 \end{pmatrix} \boldsymbol{Q} + \frac{1}{2L_u} \mathbf{\Phi}^T \mathbf{\Phi} \tag{2.24}$$

2.1.4.2 Representation of the Hamiltonian in the Fourier space

This Hamiltonian can be easily diagonalized by introducing a unitary transformation U such that

$$u_{kn} = \frac{1}{\sqrt{N}} \exp\left[\boldsymbol{i}(2k\pi n/N)\right] \tag{2.25}$$

where k, n are integers comprised between 1 and N. Applying the unitary operator U on operators Q_n and Φ_n define a new set of *non-hermitian* operators

$$\widetilde{Q}_k = \sum_{n=1}^{N} u_{kn} Q_n = \frac{1}{\sqrt{N}} \sum_{n=1}^{N} \exp\left[\boldsymbol{i}(2k\pi n/N)\right] Q_n \tag{2.26}$$

$$\widetilde{\Phi}_k = \sum_{n=1}^{N} u_{kn} \Phi_n = \frac{1}{\sqrt{N}} \sum_{n=1}^{N} \exp\left[\boldsymbol{i}(2k\pi n/N)\right] \Phi_n \tag{2.27}$$

These operators follow commutation relations of conjugate variables

$$\left[\widetilde{\Phi}_k, \widetilde{Q}^{+}_{k'}\right] = \frac{1}{N}\sum_{n=1}^{N}\sum_{m=1}^{N}\exp\left[\boldsymbol{i}(2\pi(kn-k'm)/N)\right][\Phi_n, Q_m]$$

$$= \frac{1}{N}\sum_{n=1}^{N} i\hbar\exp\left[\boldsymbol{i}(2\pi n(k-k')/N)\right] = i\hbar\delta_{kk'}$$

Indeed when $k = k'$, $\exp\left[\boldsymbol{i}(2\pi j(k-k')/N)\right] = 1$ and the sum $\sum_{n=1}^{N}\exp\left[\boldsymbol{i}(2\pi n (k-k')/N)\right]$ is equal to N, while if $k \neq k'$,

$$\sum_{n=1}^{N}\exp\left[\boldsymbol{i}(2\pi n(k-k')/N)\right] = \exp\left[\boldsymbol{i}(2\pi(k-k')/N)\right]$$

$$\left(\frac{\exp\left[\boldsymbol{i}(2\pi(k-k')\right]-1}{\exp\left[\boldsymbol{i}(2\pi(k-k')/N)\right]-1}\right) \tag{2.28}$$

$\exp\left[\boldsymbol{i}(2\pi(k-k')\right] = 1$ and thus the sum is equal to zero.

In this new basis, the non-diagonal elements of the Hamiltonian of Eq. (2.24) can be written as

$$\sum_{n=1}^{N} Q_n(Q_{n-1}+Q_{n+1}) = 2\sum_{k=1}^{N}\cos\left[2k\pi/N\right]\widetilde{Q}^{+}_{k}\widetilde{Q}_k \tag{2.29}$$

Thus, the Hamiltonian of Eq. (2.24) can be written as

$$\mathcal{H} = \sum_{k=1}^{N}\frac{2-2\cos\left[2\pi k/N\right]}{2C_u}\widetilde{Q}^{+}_{k}\widetilde{Q}_k + \frac{1}{2L_u}\widetilde{\Phi}^{+}_{k}\widetilde{\Phi}_k = \sum_{k=1}^{N}\frac{\hbar\omega_k}{2}\left(q^{+}_{k}q_k + \varphi^{+}_{k}\varphi_k\right) \tag{2.30}$$

where

$$\omega_k = \sqrt{\frac{(2-2\cos\left[2k\pi/N\right])}{L_uC_u}} \tag{2.31}$$

and

$$[\varphi_k, q^{+}_{k'}] = i\delta_{kk'} \tag{2.32}$$

2.1.4.3 Transmission Line Viewed as an External Bath

For each mode, it is possible to introduce creation and annihilation operators

$$a_k^{\rightarrow} = \frac{1}{\sqrt{2}}(\varphi_k + iq_k)$$
$$a_k^{\leftarrow} = \frac{1}{\sqrt{2}}(\varphi_k - iq_k)$$
$$(a_k^{\rightarrow})^+ = \frac{1}{\sqrt{2}}\left(\varphi_k^+ - iq_k^+\right)$$
$$(a_k^{\leftarrow})^+ = \frac{1}{\sqrt{2}}\left(\varphi_k^+ + iq_k^+\right)$$

The commutation relations of the $a_k^{\rightarrow}$ operators are such that

$$[a_k^{\rightarrow}, (a_{k'}^{\rightarrow})^+] = \delta_{kk'}$$
$$[a_k^{\leftarrow}, (a_{k'}^{\leftarrow})^+] = \delta_{kk'}$$

If N is even, the system has exactly $N/2$ different eigenenergies. Each mode is doubly degenerate and thus

$$\boxed{\mathcal{H} = \sum_{k=1}^{N/2} \hbar\omega_k \left((a_k^{\rightarrow})^+ a_k^{\rightarrow} + (a_k^{\leftarrow})^+ a_k^{\leftarrow}\right)} \tag{2.33}$$

As we increase the size Λ of the transmission line, the density of modes increases. As we decrease the size of the unit cell, the bandwidth $\sqrt{1/L_u C_u}$ increases. One can therefore safely consider that $k \ll N$ in a realistic situation. This allows to make the approximation that $\cos[x] \simeq 1 - x^2/2$ and thus

$$\omega_k \simeq \sqrt{\frac{1}{L_u C_u}} \frac{2k\pi}{N} \tag{2.34}$$

Using $\sqrt{1/L_u C_u} = \sqrt{1/\mathscr{L}\mathscr{C}u^2} = c/u$ and $\Lambda = Nu$ we get

$$\boxed{\omega_k = k.\frac{2\pi c}{\Lambda}} \tag{2.35}$$

2.1.4.4 Link Between Propagation Amplitudes and Photon Operators

The connection between the photon operators and the propagation amplitudes introduced in the previous section is directly obtained by comparing the incoming

power carried by the influx of photons with a well-defined wavevector k to the modulus of the Fourier transform of the propagation amplitude using Eq. (2.22)

$$\langle P \rangle = 2 \left| A_k^{\rightarrow} \right|^2 = \left(\frac{c}{\Lambda} \right) \hbar \omega_k \left\langle a_k^{\rightarrow +} a_k^{\rightarrow} \right\rangle$$

The expressions of $A_k^{\rightarrow}$ are thus given by

$$\boxed{A_k^{\rightarrow} = \sqrt{\frac{c}{2\Lambda} \hbar \omega_k} a_k^{\rightarrow}} \tag{2.36}$$

2.1.5 Transmission Line Resonators

In this section, we will study the use of transmission line sections with various lengths and terminations to form resonators.

2.1.5.1 Scattering Matrix

Let us consider an interface of two transmission lines with different characteristic impedance $Z_1 | Z_2$. The transmission line is separated into two separate regions, namely the left side and the right side. When an incoming wave impinges on the interface, the propagation wave amplitude can be transmitted and/or reflected partially. We thus write the scattering matrix S.

$$\begin{pmatrix} A_L^{\leftarrow} \\ A_R^{\rightarrow} \end{pmatrix} = \overbrace{\begin{pmatrix} r_{\hookleftarrow} & t_{\leftarrow} \\ t_{\rightarrow} & r_{\hookrightarrow} \end{pmatrix}}^{S} \begin{pmatrix} A_L^{\rightarrow} \\ A_R^{\leftarrow} \end{pmatrix} \tag{2.37}$$

We calculate the scattering coefficients by writing the Kirchhoff equations of voltage and current at the interface assuming $A_R^{\leftarrow} = 0$.

$$V(x^-, t) = V(x^+, t) = \sqrt{Z_1} \left(A_L^{\rightarrow} + A_L^{\leftarrow} \right) = \sqrt{Z_2} A_R^{\rightarrow}$$
$$I(x^-, t) = I(x^+, t) = \left(A_L^{\rightarrow} - A_L^{\leftarrow} \right) / \sqrt{Z_1} = \left(A_R^{\rightarrow} \right) / \sqrt{Z_2}$$

which we solve to get

$$t_{\rightarrow} = \frac{2\sqrt{Z_1 Z_2}}{Z_1 + Z_2}$$
$$r_{\hookleftarrow} = \frac{Z_2 - Z_1}{Z_1 + Z_2}$$

Similarly, two other coefficients can be established by a swap operation $Z_1 \leftrightarrow Z_2$.

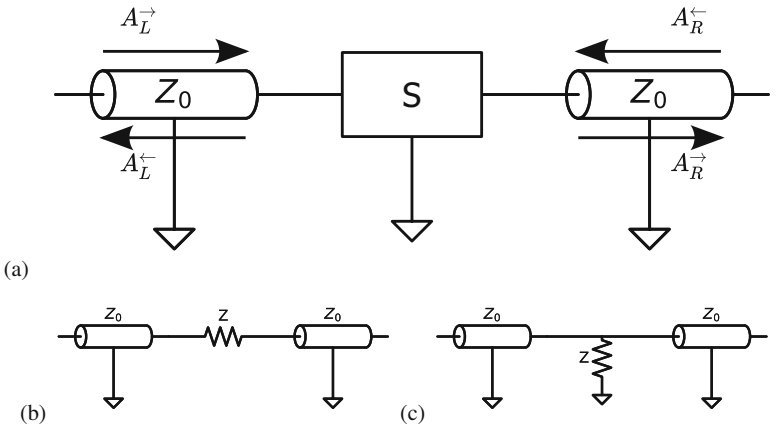

Fig. 2.5 Transmission and reflection coefficients for simple lumped elements. (**a**) Generic lumped element intersecting a transmission line. (**b**) Circuit element of impedance Z in series with the transmission line. (**c**) Circuit element of impedance Z in parallel with the transmission line

2.1.5.2 Calculating Transmission and Reflection Coefficients for Simple Lumped Elements

Let us consider the circuit described in Fig. 2.5a. The transmission line is now intersected by a lumped element system S.

For instance, we consider in Fig. 2.5b a transmission line intersected by an impedance Z in series. We get

$$
\begin{aligned}
I(x^-,t) = I(x^+,t) &= \frac{1}{\sqrt{Z_0}}\left(A_L^{\rightarrow} - A_L^{\leftarrow}\right) = \frac{1}{\sqrt{Z_0}}A_R^{\rightarrow} \\
ZI(x,t) &= V(x^-,t) - V(x^+,t) \\
&= \sqrt{Z_0}\left[\left(A_L^{\rightarrow} + A_L^{\leftarrow}\right) - A_R^{\rightarrow}\right]
\end{aligned}
$$

using the definitions of the scattering matrix, we have $A_R^{\rightarrow} = tA_L^{\rightarrow}$ and $A_L^{\leftarrow} = rA_L^{\rightarrow}$ and thus we get

$$
\boxed{\begin{aligned} r &= z/(2+z) \\ t &= 2/(2+z) \end{aligned}} \tag{2.38}
$$

with $z = Z/Z_0$. For instance, if the scatterer is a capacitor[2] $Z = 1/(-\boldsymbol{i}\omega C)$, we get

$$t = \frac{2}{2 + 1/(-\boldsymbol{i}\omega C Z_0)} \qquad r = \frac{1/(-\boldsymbol{i}\omega C Z_0)}{2 + 1/(-\boldsymbol{i}\omega C Z_0)} \tag{2.39}$$

Another interesting case to consider is a shorting circuit element as shown in Fig. 2.5c. In that case, the Kirchhoff equations gives

$$\begin{aligned} V(x^-, t) &= V(x^+, t) = \sqrt{Z_0}\left(A_L^{\rightarrow} + A_L^{\leftarrow}\right) = \sqrt{Z_0} A_R^{\rightarrow} \\ V(x^{\pm}, t) &= Z(I(x^-, t) - I(x^+, t)) \\ &= \frac{Z}{\sqrt{Z_0}}\left(A_L^{\rightarrow} - A_L^{\leftarrow}\right) - \frac{Z}{\sqrt{Z_0}} A_R^{\rightarrow} \end{aligned}$$

Thus we get

$$\boxed{\begin{aligned} r &= -1/(2z+1) \\ t &= 2z/(2z+1) \end{aligned}} \tag{2.40}$$

2.1.5.3 $\lambda/2$ Resonators with Symmetrical Terminations

The use of symmetrical terminations on both ends of a segment of length $L_{res} = \lambda/2$ ensures that exactly at the resonant frequency $\omega_r = \pi c/L_{res}$, a continuous wave signal is fully transmitted, and no reflection is observed. This results from coherent interference of transmission amplitudes which converges to a unitary transmission coefficient

$$\tau = \sum_{j=0}^{\infty} t e^{\boldsymbol{i} k L_{res}} \left(r^2 e^{2\boldsymbol{i} k L_{res}}\right)^j t = e^{\pi \boldsymbol{i}\omega/\omega_r} \sum_{j=0}^{\infty} t^2 \left(r^2 e^{2\pi \boldsymbol{i}\omega/\omega_r}\right)^j \tag{2.41}$$

$$\tau = \frac{t^2 e^{\pi \boldsymbol{i}\omega/\omega_r (1+\boldsymbol{i}/Q_{int})}}{1 - r^2 e^{2\pi \boldsymbol{i}\omega/\omega_r (1+\boldsymbol{i}/Q_{int})}} \tag{2.42}$$

where $kL_{res} = \frac{\omega}{c}(1 + \boldsymbol{i}/Q_{int}) \times L_{res} = \pi \frac{\omega}{\omega_r}(1 + \boldsymbol{i}/Q_{int})$, Q_{int} representing the internal quality factor due to internal losses in the resonator.

[2] We adopt the quantum convention for wave propagation (i.e. $e^{\boldsymbol{i}(kx-\omega t)}$), which differs by a sign from the one found typically in the microwave textbooks (i.e. $e^{\boldsymbol{i}(\omega t - kx)}$).

An identity can be established relating the round trip frequency $\omega_r/2\pi$, the transmission coefficient, and the energy leakage κ via the ports

$$\kappa = 2 \cdot \omega_r/2\pi \cdot |t|^2 \tag{2.43}$$

The factor 2 stems from the fact that two scattering events occur per round trip. We thus get

$$\boxed{Q_{ext} = {}^{\omega_r}/_{\kappa} = \pi/|t|^2} \tag{2.44}$$

For instance, if the scatterer is a capacitor of capacitance C, we obtain from Eq. (2.39), $|t|^2 \simeq 4C^2\omega_r^2 Z_0^2$ and thus

$$Q_{ext} = \frac{\pi}{4C^2\omega_r^2 Z_0^2} \tag{2.45}$$

In Fig. 2.6a, b, we represented the frequency dependence of the amplitude of the transmitted field $|\tau|$ and of its relative phase. When $Q_{int} = +\infty$ (blue curve), the transmission at $\omega = \omega_r$ is equal to one:

$$|\tau(\omega_r)| = \frac{|t^2|}{|1 - r^2|} \simeq 1 \tag{2.46}$$

The phase shifts by π at resonance. As one increases the ratio Q_{ext}/Q_{int}, the maximum transmission at resonance decreases (red and green curves).

2.1.5.4 $\lambda/4$ Resonators with Short Circuit Termination

Another important type of transmission line resonator is the so-called $\lambda/4$ resonator. In this type of resonator, the segment length $L_{res} = \lambda/4$ and is terminated by a short circuit, such that at the resonant frequency $\omega_r = \pi c/(2 * L_{res})$, a phase shift is observed in the reflection of the signal. This results from coherent interference of reflection amplitudes

$$\begin{aligned}\rho &= r - t^2 e^{2\boldsymbol{i}kL_{res}} \sum_{j=0}^{\infty} (-1)^j \left(r e^{2\boldsymbol{i}kL_{res}}\right)^j \\ &= r - e^{\pi \boldsymbol{i}\omega/\omega_r(1+\boldsymbol{i}/Q_{int})} \frac{t^2}{1 + r e^{\pi \boldsymbol{i}\omega/\omega_r(1+\boldsymbol{i}/Q_{int})}}\end{aligned} \tag{2.47}$$

where $2kL_{res} = \frac{\omega}{c}(1 + \boldsymbol{i}/Q_{int}) \times L_{res} = \pi \frac{\omega}{\omega_r}(1 + \boldsymbol{i}/Q_{int})$.

The energy leakage κ via the port is related to the round trip frequency $\omega_r/2\pi$ and to the transmission coefficient by

$$\kappa = \omega_r/2\pi \cdot |t|^2 \tag{2.48}$$

We thus get

$$\boxed{Q_{ext} = {}^{\omega_r}/_{\kappa} = 2\pi/\,|t|^2} \tag{2.49}$$

Depending on the ratio between Q_{int} and Q_{ext},we can define three regimes characterized by different behavior of the reflexion coefficent ρ.

The *overcoupled regime* (blue curve) occurs when $Q_{ext} << Q_{int}$. In this regime, $|\rho| \sim 1$ for all frequencies. However, the phase of ρ changes abruptly close to multiples of the resonance frequency and undergoes a 2π shift as shown in Fig. 2.6.

The *critical coupling* (green curve) occurs when $Q_{ext} = Q_{int}$. For this regime, the amplitude reaches almost zero at resonance, while a discontinuity in the phase brings a phase shift of π.

The undercoupled regime (red curve) occurs when $Q_{ext} > Q_{int}$. In this regime, the resonance corresponds to a dip in the amplitude of ρ and a shift $< \pi$ in its phase. The undercoupled resonator is particularly difficult to measure in reflexion since both the amplitude and the phase differs slightly from the out-of-resonance value.

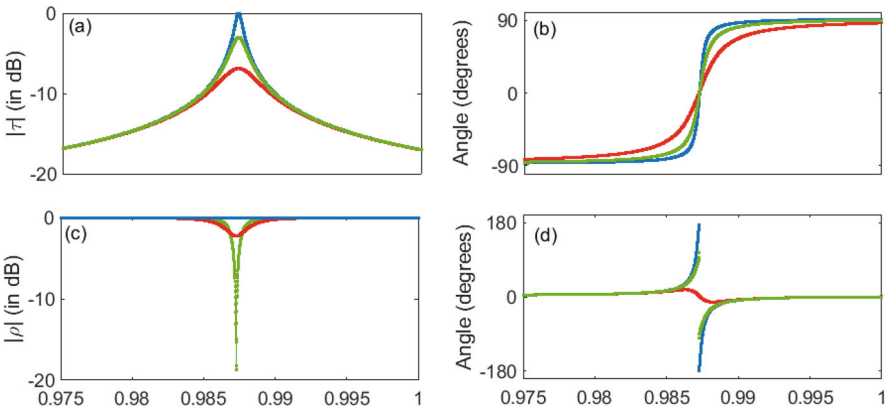

Fig. 2.6 (**a–b**) Modulus of the transmitted field $|\tau|$ and relative phase of the output field via a $\lambda/2$ resonator with symmetrical terminations ($z = 50\,\boldsymbol{i}$, $Q \sim 2000$) assuming no internal losses ($Q_{in} = +\infty$, blue curve) or internal losses of quality factor $Q_{in} = 4000$ (green curve) and $Q_{in} = 1000$ (red curve). (**c–d**) Modulus of the reflected field $|\rho|$ and relative phase of the reflected field on a $\lambda/4$ resonator with short circuit termination ($z = 50\,\boldsymbol{i}$, $Q \sim 4000$) assuming no internal losses ($Q_{in} = +\infty$, blue curve) or internal losses of quality factor $Q_{in} = 4000$ (critical coupling regime, green curve) and $Q_{in} = 1000$ (red curve)

2.1.5.5 Expression for the Local Current and/or Voltage in the Resonator as a Function of Propagation Wave Amplitudes

One can write the current/voltage at a given position in the resonator as a linear response of the propagation wave amplitudes of incoming waves $A_L^{\rightarrow}$ and $A_R^{\leftarrow}$ on both side of the resonator. The obtained linear map can be summarized as

$$I(x,\omega) = \frac{1}{\sqrt{Z_0}}\left(f_{\rightarrow}(\omega,x)\,A_L^{\rightarrow} + f_{\leftarrow}(\omega,x)\,A_R^{\leftarrow}\right) \tag{2.50}$$

$$V(x,\omega) = \sqrt{Z_0}\left(g_{\rightarrow}(\omega,x)\,A_L^{\rightarrow} + g_{\leftarrow}(\omega,x)\,A_R^{\leftarrow}\right) \tag{2.51}$$

The exact numerical value of $f_{\rightarrow/\leftarrow}$ and $g_{\rightarrow/\leftarrow}$ can be calculated by considering the coherent interference from the scattering of all the elements . In the case of a symmetric $\lambda/2$ resonator, we obtain

$$\begin{aligned} f_{\rightarrow}(\omega,x) &= t\frac{e^{i\mathbf{k}\mathbf{x}} - re^{i\mathbf{k}(2L_{res}-\mathbf{x})}}{1-e^{i\mathbf{k}L_{res}}r^2} \\ f_{\leftarrow}(\omega,x) &= t\frac{e^{i\mathbf{k}(L_{res}-\mathbf{x})} - re^{i\mathbf{k}(L_{res}+\mathbf{x})}}{1-e^{i\mathbf{k}L_{res}}r^2} \end{aligned} \tag{2.52}$$

similarly for the voltage, we get

$$\begin{aligned} g_{\rightarrow}(\omega,x) &= t\frac{e^{i\mathbf{k}\mathbf{x}} + re^{i\mathbf{k}(2L_{res}-\mathbf{x})}}{1-e^{i\mathbf{k}L_{res}}r^2} \\ g_{\leftarrow}(\omega,x) &= t\frac{e^{i\mathbf{k}(L_{res}-\mathbf{x})} + re^{i\mathbf{k}(L_{res}+\mathbf{x})}}{1-e^{i\mathbf{k}L_{res}}r^2} \end{aligned}$$

2.1.6 Quantization of Transmission Line Resonators

2.1.6.1 $\lambda/2$ Resonators with Open Circuit Terminations

Let us first consider a transmission line resonator of length L_{res} with open circuit termination on both sides. Contrary to a lumped-element resonator, such a distributed resonator possesses an infinite number of modes. The characteristic impedance of the resonator is given by $Z_0 = \sqrt{\mathscr{L}/\mathscr{C}}$ where $\mathscr{C}$ is the capacitance per unit length and $\mathscr{L}$ the inductance per unit length. We introduce the flux $\Phi(\mathbf{x})$ such that $V = \partial_t \Phi$ at position $\mathbf{x} \in [0, L_{res}]$. The Lagrangian writes as follows:

$$\mathcal{L} = \frac{1}{2}\int_0^{L_{res}} \left(\mathscr{C}V^2 - \mathscr{L}I^2\right) d\mathbf{x} = \frac{1}{2}\int_0^{L_{res}} \left(\mathscr{C}\dot{\Phi}^2 - \frac{1}{\mathscr{L}}\left(\partial_x \Phi\right)^2\right) d\mathbf{x} \tag{2.53}$$

Taking into account the boundary condition, it is possible to decompose $V(\mathbf{x})$ and $I(\mathbf{x})$ into an infinite number of stationary wave modes. We thus decompose Φ into infinite stationary modes of mode number j, each verifying the open circuit

boundary condition $I = 0$ at $\mathbf{x} = 0$ and $\mathbf{x} = L_{res}$, we thus write

$$\Phi(\mathbf{x}) = \sum_{j=1}^{\infty} \Phi_j \cos\left(\pi j \mathbf{x}/L_{res}\right) \tag{2.54}$$

which we inject into the Lagrangian expression and get

$$\mathcal{L} = \frac{L_{res}}{2} \sum_{j=1}^{\infty} \left(\frac{\mathscr{C}}{2} \dot{\Phi}_j^{\,2} - \frac{1}{2\mathscr{L}} \left(\frac{\pi j}{L_{res}} \Phi_j \right)^2 \right) \tag{2.55}$$

We obtain the Hamiltonian after performing the Legendre transformation

$$\mathcal{H} = \sum_{j=1}^{\infty} \mathcal{H}_j = \frac{1}{L_{res}} \sum_{j=1}^{\infty} \left(\frac{Q_j^2}{\mathscr{C}} + \frac{\pi^2 j^2}{4\mathscr{L}} \Phi_j^2 \right) \tag{2.56}$$

where $Q_j = \partial \mathcal{L} / \partial \dot{\Phi}_j = \mathscr{C} L_{res} \dot{\Phi}_j / 2$ is the conjugated variable of Φ_j such that $\left[\Phi_i, Q_j\right] = i\hbar\delta_{ij}$. We can further simplify the Hamiltonian by introducing creation and annihilation operators for each mode

$$\mathcal{H}_j = \hbar\omega_j \left(a_j^{\dagger} a_j + 1/2 \right) \tag{2.57}$$

where $a_j = \sqrt{\frac{j\pi}{4Z_0\hbar}} \Phi_j + i \sqrt{\frac{Z_0}{j\hbar\pi}} Q_j$, $\omega_j = j\omega_r = j\left(\frac{\pi}{L_{res}} c\right)$ and $c = \sqrt{\frac{1}{\mathscr{C}\mathscr{L}}}$ the wave velocity. Using $I(\mathbf{x}) = -\partial_x \Phi(\mathbf{x}) / \mathscr{L}$, we get

$$I(\mathbf{x}) = \sum_{j=1}^{\infty} \overbrace{\delta I_0 \sqrt{j} \sin\left(\pi j x / L_{res}\right)}^{\delta I_j(x)} \left(a_j + a_j^{\dagger} \right) \tag{2.58}$$

where $\delta I_0 = \omega_r \sqrt{\frac{\hbar}{\pi Z_0}}$. Similarly, using $V(\mathbf{x}) = \dot{\Phi}(\mathbf{x})$, we get

$$V(\mathbf{x}) = -\boldsymbol{i} \sum_{j=1}^{\infty} \overbrace{\delta V_0 \sqrt{j} \cos\left(\pi j x / L_{res}\right)}^{\delta V_j(x)} \left(a_j - a_j^{\dagger} \right) \tag{2.59}$$

where $\delta V_0 = \omega_r \sqrt{\frac{\hbar Z_0}{\pi}}$.

2.1.6.2 Determining the Current Operator by Filter Function Formalism

Using Eqs. (2.50) and (2.36) we get that

$$\hat{I}(x) = \sqrt{\frac{c}{2\Lambda}} \sum_k \sqrt{\frac{\hbar\omega_k}{Z_0}} \left(f_{\rightarrow}(\omega_k, x)\, a^{\rightarrow}_{L,k} + f_{\leftarrow}(\omega_k, x)\, a^{\leftarrow}_{R,k} \right) + \text{H.c.} \tag{2.60}$$

Let us introduce a new operator $\mathbf{A}$ as a linear combination of $a^{\rightarrow}_{L,k}$ and $a^{\leftarrow}_{R,k}$

$$\mathbf{A} = \frac{\sum_k \sqrt{k} \left(f_{\rightarrow}(\omega_k, x)\, a^{\rightarrow}_{L,k} + f_{\leftarrow}(\omega_k, x)\, a^{\leftarrow}_{R,k} \right)}{\sqrt{\sum_k k \left(|f_{\rightarrow}(\omega_k, x)|^2 + |f_{\leftarrow}(\omega_k, x)|^2 \right)}} \tag{2.61}$$

which verifies $\left[\mathbf{A}, \mathbf{A}^{\dagger}\right] = 1$ and can rewrite the current operator under the form

$$\hat{I}(x) = \delta I(x) \left(\mathbf{A} + \mathbf{A}^{\dagger} \right)$$

where

$$\delta I(x) = \sqrt{\sum_k \frac{c}{2\Lambda Z_0} \hbar\omega_k \left(|f_{\rightarrow}(\omega_k, x)|^2 + |f_{\leftarrow}(\omega_k, x)|^2 \right)}$$

For convenience, we introduce the density of states

$$\eta(\omega) \equiv \frac{1}{\Delta\omega} = \Lambda / 2\pi c \tag{2.62}$$

Injecting the expression of η we obtain an expression independent of Λ

$$\boxed{\delta I(x) = \sqrt{\int_{d\omega} \frac{\hbar\omega}{4\pi Z_0} \left(|f_{\rightarrow}|^2(\omega, x) + |f_{\leftarrow}|^2(\omega, x) \right)}} \tag{2.63}$$

2.2 Superconducting Qubits

2.2.1 Using the Non-linearity of Josephson Junctions

A circuit formed by linear components, such as capacitors and inductors, behaves as an harmonic oscillator and not as a qubit. A non-linear element is therefore essential in order to differentiate the transitions between states $|0\rangle$ and $|1\rangle$ from other higher-lying eigenstates transitions. In superconducting circuits, this non-linearity is obtained by adding to the circuit one or several Josephson junctions. Josephson

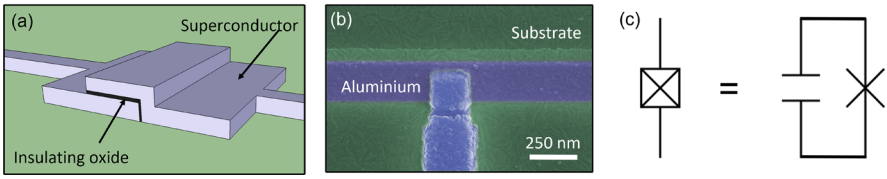

Fig. 2.7 The Josephson junction: a non-linear, non-dissipative element. (**a**) Schematic representation of a Josephson junction showing two superconducting layers separated by a thin insulating oxide layer (**b**) Colored SEM micrograph showing a Josephson junction. (**c**) Circuit diagram representing a Josephson junction, which corresponds to a capacitor of capacitance C_J in parallel with a Josephson (non linear) inductor of inductance $L_J = \frac{\varphi_0}{I_0}$ and represented as a cross

junctions are formed by two superconducting islands separated by a thin insulating layer (see Fig. 2.7) that allows tunneling of Cooper pairs. They are characterized by the so-called Josephson relations:

$$\boxed{\begin{aligned} I &= I_0 \sin\left(\frac{\Phi}{\varphi_0}\right) \\ V &= \dot{\Phi} \end{aligned}} \tag{2.64}$$

where Φ is the flux threading the junction, I_0 is the critical current of the junction and $\varphi_0 = \hbar/2e$ is the reduced magnetic flux quantum.

Josephson junctions are almost non-dissipative. This property allows their use in quantum circuits. The potential energy of the Josephson junction is given by:

$$E = \int_{-\infty}^{t} I(t)V(t)dt = \int_{-\infty}^{t} I_0 \sin\left(\frac{\Phi}{\varphi_0}\right)\dot{\Phi}dt = -E_J \cos(\frac{\Phi}{\varphi_0}) \tag{2.65}$$

where E_J=$I_0\varphi_0$ is called **Josephson energy**.

2.2.2 The Charge Qubit

The simplest version of superconducting qubit, also called Cooper pair box (CPB) consists of two superconducting islands connected by a single Josephson junction of capacitance C_J and Josephson energy E_J. One of the island is electrostatically biased by a voltage source V_g in series with a capacitor C_g. The Cooper pair box was initially developped in 1996 by the Quantronics group at CEA Saclay [6] . In 1999, a team from NEC used the CPB to demonstrate for the first time a coherent superposition of states [7].

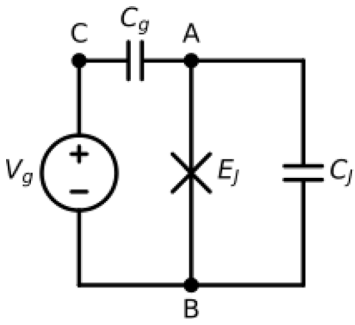

Fig. 2.8 Circuit schematic of a Cooper Pair Box (CPB). The device consists of a Josephson junction with Josephson energy E_J and capacitance C_J, capacitively coupled to a voltage source V_g through a gate capacitor C_g

2.2.2.1 Solving the Cooper Pair Box Hamiltonian

In Fig. 2.8, we present a circuit schematic of a CPB. The points A, B and C are nodes of the circuit and are characterized by electrical potentials V_A,V_B and V_C. We define a spanning tree by choosing the flux Φ connecting nodes A and B.

The inductive energy U is simply given by Eq. (2.65)

$$U = -E_J \cos(\frac{\Phi}{\varphi_0}) \tag{2.66}$$

The capacitive energy K of the system is given by

$$K = \frac{1}{2} C_J (V_A - V_B)^2 + \frac{1}{2} C_g (V_A - V_C)^2$$

Using the definitions $\dot{\Phi} = V_A - V_B$ and $V_g = V_C - V_B$, it is possible to express V_A,V_B and V_C as a function of $\dot{\Phi}$ and V_g, such that

$$K = \frac{1}{2} C_J \dot{\Phi}^2 + \frac{1}{2} C_g \left(\dot{\Phi} - V_g\right)^2 \tag{2.67}$$

It is thus possible to write the Lagrangian $\mathcal{L}$ as

$$\mathcal{L} = \frac{1}{2} C_J \dot{\Phi}^2 + \frac{1}{2} C_g \left(\dot{\Phi} - V_g\right)^2 + E_J \cos(\frac{\Phi}{\varphi_0}) \tag{2.68}$$

The conjugate momentum of our system is given by

$$Q \equiv \frac{\partial \mathcal{L}}{\partial \dot{\Phi}} = (C_J + C_g)\dot{\Phi} - C_g V_g \tag{2.69}$$

and the Hamiltonian is thus given by

$$\mathcal{H} = \dot{\Phi} Q - \mathcal{L} = \frac{1}{2(C_g + C_J)} (Q + C_g V_g)^2 - E_J \cos(\frac{\Phi}{\varphi_0}) - \frac{1}{2} C_g V_g^2 \tag{2.70}$$

By dropping the constant term and introducing the new variables $n = \frac{Q}{2e}$ and $\varphi = \frac{\Phi}{\varphi_0}$ such that $[\varphi, n] = \frac{1}{\hbar}[\Phi, Q] = \boldsymbol{i}$, we can write the Hamiltonian as

$$\boxed{\mathcal{H} = 4E_C(\hat{n} - n_g)^2 - E_J \cos(\hat{\varphi})} \tag{2.71}$$

where $n_g = -\frac{C_g V_g}{2e}$ and $E_C = \frac{e^2}{2(C_J + C_g)}$. In order to find the eigenenergies and corresponding eigenstates, the Hamiltonian can be represented in the basis formed by the eigenstates $|n\rangle$ of operator $\widehat{n}$. Indeed, $[\varphi, n] = \boldsymbol{i}$ implies that $\langle\varphi|n\rangle = e^{\boldsymbol{i}n\varphi}$ and thus, the operator $\cos(\hat{\varphi}) = 1/2(e^{\boldsymbol{i}\hat{\varphi}} + e^{-\boldsymbol{i}\hat{\varphi}})$ can be written in the eigenbasis $|n\rangle$ as

$$\cos(\hat{\varphi})\,|n\rangle = \frac{1}{2}(e^{\boldsymbol{i}\hat{\varphi}} + e^{-\boldsymbol{i}\hat{\varphi}}) \sum |\varphi\rangle\,\langle\varphi|n\rangle = \frac{1}{2}\left(|n+1\rangle + |n-1\rangle\right) \tag{2.72}$$

It is thus easy to represent the Hamiltonian in a truncated charge basis as

$$H = \begin{pmatrix} 4E_C(-2-n_g)^2 & -E_J/2 & 0 & 0 & 0 \\ -E_J/2 & 4E_C(-1-n_g)^2 & -E_J/2 & 0 & 0 \\ 0 & -E_J/2 & 4E_C(0-n_g)^2 & -E_J/2 & 0 \\ 0 & 0 & -E_J/2 & 4E_C(1-n_g)^2 & -E_J/2 \\ 0 & 0 & 0 & -E_J/2 & 4E_C(2-n_g)^2 \end{pmatrix} \tag{2.73}$$

The choice of the truncation size depends on the parameters E_J and E_C and on the precision which is required. The results of such a diagonalization for the ground and first excited states are shown in Fig. 2.9 for different ratios of E_J/E_C. The voltage V_g allows controlling the transition energy of the qubit. As can be

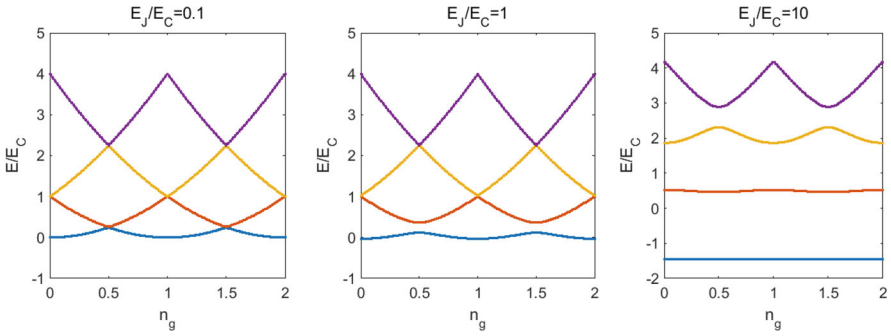

Fig. 2.9 First four energy levels of the Cooper pair box as a function of the reduced gate charge n_g for E_J/E_c ratios equal to 0.1, 1 and 10 (left to right). As can be seen, for $E_J \gg E_c$, the charge dispersion curves becomes more and more flat

seen, the charge-dispersion curve of the first two levels becomes almost flat when $E_J \gg E_c$.

2.2.2.2 The Split Cooper Pair Box

It is possible to get some additionnal control of the qubit energy by replacing the Josephson junction of the CPB by a Superconducting Quantum Interference Device (SQUID) [1]. In the following section we will show how the SQUID allows controlling the qubit transition energy via the magnetic flux Φ_S threading its loop. First, let us write the potential energy U_S of the SQUID, shown in Fig. 2.10:

$$U_S = -\frac{1+d}{2} E_J \cos(\varphi_1) - \frac{1-d}{2} E_J \cos(\varphi_2) \tag{2.74}$$

where d is the asymmetry parameter ,which can get any value in range of [0, 1]. A DC magnetic flux Φ_S is threading the loop of the SQUID such that $\varphi_1 - \varphi_2 = \frac{\Phi_S}{\varphi_0}$ leading to:

$$U_S = \underbrace{-E_J \sqrt{\frac{\left(1+d^2\right) + \left(1-d^2\right)\cos\left(\frac{\Phi_s}{\varphi_0}\right)}{2}}}_{-E_J(\Phi_S, d)} \cdot \cos\left(\frac{\varphi_1+\varphi_2}{2} + \arctan\left[-d \cdot \tan\left(\frac{\Phi_S}{2\varphi_0}\right)\right]\right) \tag{2.75}$$

The potential energy of the SQUID is therefore equivalent to the potential energy of a *single* Josephson junction with tunable Josephson energy $E_J(\Phi_S, d)$ that varies between dE_J to E_J. When the asymmetry is large ($d \simeq 1$), the Josephson energy of the SQUID varies slightly and thus is less sensitive than for a symmetric SQUID ($d = 0$).

The remaining part of the quantization process proceeds as before, yielding an Hamiltonian of the split Cooper pair box of the form

$$\mathcal{H} = 4E_C(\hat{n} - n_g)^2 - E_J(\Phi_S, d)\cos\left(\hat{\varphi} + \gamma(\Phi_S, d)\right) \tag{2.76}$$

where $\gamma(\Phi_S, d) = \arctan\left[-d \cdot \tan\left(\frac{\Phi_s}{2\varphi_0}\right)\right]$.

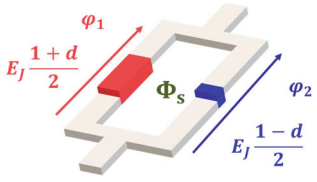

Fig. 2.10 Schematic of an asymmetric SQUID

2.2.2.3 The Transmon Qubit

The transmon qubit has been developed in 2006 in the group of R. Schoelkopf at Yale [8]. It is a CPB whose charging energy is strongly reduced by putting a large capacitance in parallel to the Josephson junction, such that the device is in the regime $E_J \sim 100\, E_C$. As shown in Fig. 2.11b, the charge dispersion of the energy levels of the CPB, $\Delta\omega(n_g)$, becomes extremely weak and the transition energy $\hbar\omega_{01}$ almost insensitive to the value of the gate charge n_g. This reduced sensitivity to charge is highly advantageous in experiments since it makes the qubit almost insensitive to charge noise and thus increases the coherence time. However, when increasing the ratio E_J/E_C one also reduces the anharmonicity $\alpha = (\omega_{12} - \omega_{01})/\omega_{01}$ (see Fig. 2.11a), therefore limiting the speed of gate operations that can be realized with this qubit (Fig. 2.11b).

The Hamiltonian of the system is similar to Eq. (2.71). Yet, the high E_J/E_C ratio reduces strongly the flux fluctuations and one can thus develop the cosine function close to zero as $\cos(\hat{\varphi}) = 1 - \frac{1}{2}\hat{\varphi}^2 + \frac{1}{4!}\hat{\varphi}^4 + O\left(\hat{\varphi}^6\right)$.

When taking only into account the terms in $\hat{\varphi}^2$, the system behaves as an harmonic oscillator of frequency $\hbar\omega_r = \sqrt{8E_J E_C}$. It is possible to express the operators $\widehat{n}$ and $\hat{\varphi}$ as a function of the creation and annihilation operator a and a^+

$$\hat{\varphi} = \left(\frac{2E_C}{E_J}\right)^{1/4}\left(a + a^+\right)$$

$$\widehat{n} = -\frac{i}{2}\left(\frac{E_J}{2E_C}\right)^{1/4}\left(a - a^+\right)$$

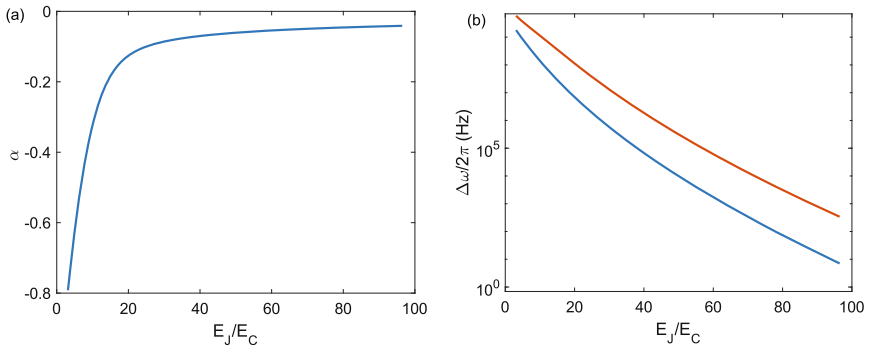

Fig. 2.11 Transmon Properties. (**a**) Anharmonicity $\alpha = (\omega_{12} - \omega_{01})/\omega_{01}$ versus E_J/E_C ratio. (**b**) Amplitude of the charge dispersion $\Delta\omega = \omega(n_g = 0.5) - \omega(n_g = 0)$ versus E_J/E_C for the $0 \rightarrow 1$ transition (in blue) and $1 \rightarrow 2$ transition (in red). The $0 \rightarrow 1$ transition frequency of the qubit is kept around 4.8 GHz

The zero point fluctuations of the phase operator, $\Delta\varphi = \left(\frac{2E_C}{E_J}\right)^{1/4}$, are small when $E_J \gg E_C$, which justifies our approximation a posteriori. Developing the cosine potential to higher order gives

$$\boxed{\mathcal{H} = \hbar\omega_r \left(a^+ a + \frac{1}{2}\right) - \frac{E_C}{12}\left(a + a^+\right)^4} \tag{2.77}$$

The second term of the Hamiltonian can be viewed as a Kerr non-linearity. It can be solved perturbatively using first order perturbation theory. The shift of the n^{th} energy level of the harmonic oscillator is given by

$$\begin{aligned} \Delta E_n &= \left\langle n \left| -\frac{E_C}{12}\left(a + a^+\right)^4 \right| n \right\rangle \\ &= -\frac{E_C}{12}\left(6n^2 + 6n + 3\right) \end{aligned} \tag{2.78}$$

and thus $\Delta E_{n+1} - \Delta E_n = -E_C(n+1)$. The Kerr non-linear term modifies the equidistant interlevel spacing and defines a qubit with anharmonicity

$$\alpha = (\omega_{12} - \omega_{01})/\omega_{01} = -\sqrt{E_C/8E_J} \tag{2.79}$$

2.2.2.4 Improving Transmon Design

Typical values for a transmon are $E_C/h = 200$ MHz and $E_J/h = 15$ GHz giving a ratio $E_J/E_C = 75$, a qubit frequency $\omega_{01}/2\pi = 4.7$ GHz and an anharmonicity $\alpha = -0.04$. As mentioned earlier, the low anharmonicity requires that the gate time should be much longer than $h/E_c = 5$ ns.

The typical relaxation times of transmons have been largely improved by the introduction of three dimensional cavity, which reduce the impact of dielectric losses in the circuit [9]. Various works have tried to reduce these losses in order to increase the fidelity of the qubit while keeping a 2D scalable architecture [10, 11]. This can be done by reducing the interface defects between the metal and the substrate [11]. In recent works [12], transmons with typical relaxation time of $T_1 \sim 50\ \mu$s are controlled by ~ 40 ns two qubit gates, leading to two qubit gate fidelity in the range of 99.3–99.8%.

2.2.3 The Superconducting Flux Qubit

The superconducting flux qubit is a superconducting circuit which consists of a micron-size superconducting aluminum loop intersected by three (or more) Josephson junctions, among which one of the junctions is smaller than the others by a factor α (see Fig. 2.12). This qubit was initially developed at Delft University in 1999 [13–17].

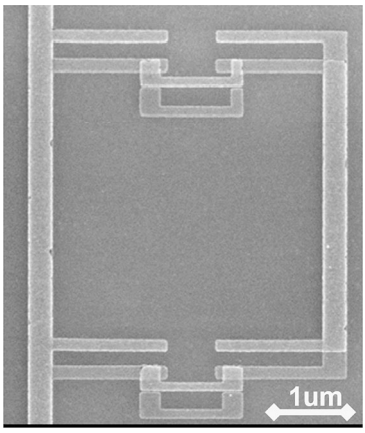

Fig. 2.12 Scanning Electron Microscope (SEM) image of a 4-junction flux qubit

2.2.3.1 Potential Energy of a Flux Qubit

The potential energy of the circuit can be written as a sum of the potential energies of each junction intersecting the loop (see Eq. (2.65)). A DC magnetic flux Φ is threading the loop, therefore due to Faraday law $\sum_{i=1}^{n-1} \varphi_i + \varphi_\alpha = \frac{\Phi}{\varphi_0}$ and thus:

$$U = -E_J \left[\sum_{i=1}^{n-1} \cos(\varphi_i) + \alpha \cos(\frac{\Phi}{\varphi_0} - \sum_{i=1}^{n-1} \varphi_i) \right] \tag{2.80}$$

For a flux qubit with $n = 3$ junctions, the potential energy can be plotted with a pseudo-color plot shown in Fig. 2.13.

When $\Phi/\varphi_0 = \pi$ and for $\alpha > \alpha_{min}$, the potential energy U exhibits two degenerated minima (Fig. 2.13), the potential barrier between these two minima being a function of the parameters of the junctions. The position of the minima are given by solving the partial derivative equations $\partial_{\varphi_i} U = 0$. The two solutions verify the simple equation

$$\sin \varphi^* = \alpha \sin\left((n-1)\varphi^*\right) \tag{2.81}$$

and correspond to two opposite persistent currents $I_P = \pm I_0 \sin \varphi^*$ flowing in the loop.

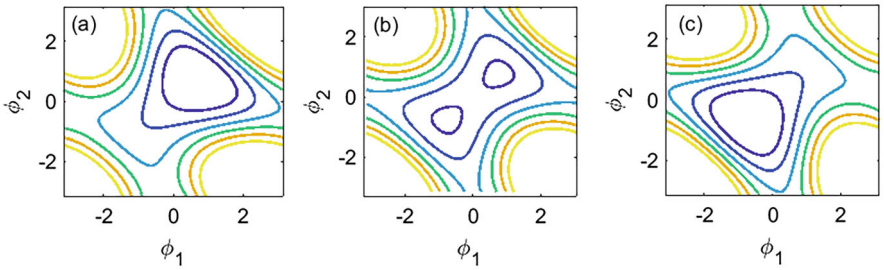

Fig. 2.13 Potential energy landscape of a 3-island flux qubit with parameters $\alpha = 0.7$. (**a**) for $\Phi/\varphi_0 = 0.8\pi$; (**b**) for $\Phi/\varphi_0 = \pi$; (**c**) for $\Phi/\varphi_0 = 1.2\pi$

By inverting this equation, we find that $U_{n-2}(\cos\varphi^*) = \frac{1}{\alpha}$ and

$$\boxed{I_P = \pm I_0\sqrt{1 - \left[U_{n-2}^{-1}\left(\frac{1}{\alpha}\right)\right]^2}} \tag{2.82}$$

where U_{n-2} is the (n-1)-th Chebyshev polynomial of the second kind. The following table summarizes the common values for $n = 3, 4$ or 5.

n	U_{n-2}	$\lvert I_P\rvert$	α_{min}
3	$2X$	$I_0\sqrt{1-\left(\frac{1}{2\alpha}\right)^2}$	$\frac{1}{2}$
4	$4X^2-1$	$I_0\sqrt{\frac{3}{4}-\frac{1}{4\alpha}}$	$\frac{1}{3}$
5	$8X^3-4$	$I_0\sqrt{1-\left(\frac{1}{2}+\frac{1}{8\alpha}\right)^{2/3}}$	$\frac{1}{4}$

2.2.3.2 Kinetic Energy of a Flux Qubit

For a 4-junction qubit, the kinetic energy K of the system is the sum of the capacitive energies of the circuit shown in Fig. 2.14

$$K = \frac{1}{2}\sum_{i\neq j} C_{ij}\left(V_j - V_i\right)^2 \tag{2.83}$$
$$+\frac{1}{2}C_J\left((V_1-V_2)^2 + (V_2-V_3)^2 + (V_3-V_4)^2 + \alpha\,(V_4-V_1)^2\right)$$

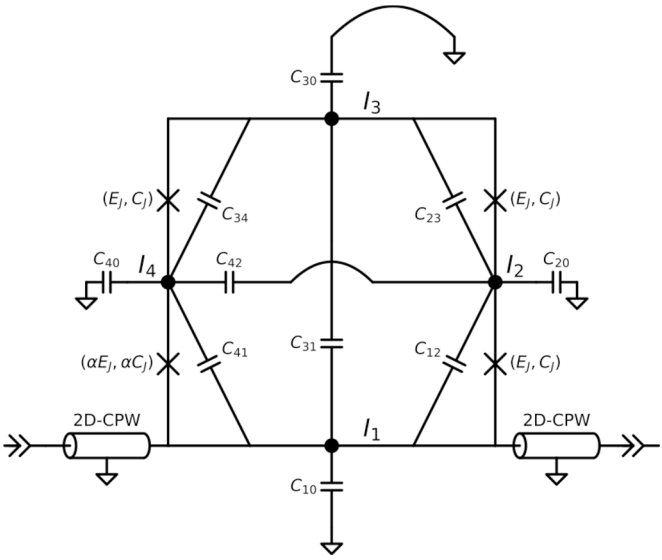

Fig. 2.14 Equivalent circuit diagram of a flux qubit. The Josephson junctions are defined by their Josephson energy E_J and their bare capacitance C_J. The island I_1 is galvanically connected to a coplanar waveguide resonator. Each island is capacitively coupled to its surrounding by geometric capacitances denoted as C_{ij} where $(i, j) \in (0, 1, .., 4)$, the index 0 representing the ground

It is a quadratic form of the island voltages V_i and can thus be written as

$$K = \frac{1}{2}\mathbf{V}^T\mathbf{C}\mathbf{V} \tag{2.84}$$

where $\mathbf{V^T} = \left(V_1\ , V_2\ , V_3,\ V_4\right)$ and $\mathbf{C}$ is a 4×4 matrix which we will refer in the following as the capacitance matrix. The matrix $\mathbf{C}$ can be written as the sum of the Josephson capacitance matrix $\mathbf{C_J}$ and the geometric capacitance matrix $\mathbf{C_{geom}}$.

$$\mathbf{C} = \mathbf{C_J} + \mathbf{C_{geom}} \tag{2.85}$$

where

$$\mathbf{C_J} = C_J \begin{pmatrix} 1+\alpha & -1 & 0 & -\alpha \\ -1 & 2 & -1 & 0 \\ 0 & -1 & 2 & -1 \\ -\alpha & 0 & -1 & 1+\alpha \end{pmatrix} \tag{2.86}$$

and

$$\mathbf{C_{geom}} = \begin{pmatrix} C_{10} & 0 & 0 & 0 \\ 0 & C_{20} & 0 & 0 \\ 0 & 0 & C_{30} & 0 \\ 0 & 0 & 0 & C_{40} \end{pmatrix} + \begin{pmatrix} \sum_{j\neq 1} C_{1j} & -C_{12} & -C_{13} & -C_{14} \\ -C_{21} & \sum_{j\neq 2} C_{2j} & -C_{23} & -C_{24} \\ -C_{31} & -C_{32} & \sum_{j\neq 3} C_{3j} & -C_{34} \\ -C_{41} & -C_{42} & -C_{43} & \sum_{j\neq 4} C_{4j} \end{pmatrix} \tag{2.87}$$

2.2.3.3 Legendre Transformation and Hamiltonian

The Lagrangian of the system is $\mathcal{L} = K - U$. The conjugate momenta of our system are given by

$$n_j \equiv \frac{1}{\hbar}\frac{\partial \mathcal{L}}{\partial \dot{\varphi}_j} \tag{2.88}$$

Since $\frac{\Phi_0}{2\pi}\dot{\varphi}_j, = V_{j+1} - V_j$, it is necessary to express the kinetic energy terms in a new basis. Since island I_1 shown in Fig. 2.14 is galvanically connected to the central conductor of a CPW, we can safely assume that $V_1 = 0\,\mathrm{V}$, which simplifies considerably the transformation:

$$\begin{aligned} V_1 &= 0 \\ V_2 &= \cancelto{0}{V_1} + V_{12} \\ V_3 &= \cancelto{0}{V_1} + V_{12} + V_{23} \\ V_4 &= \cancelto{0}{V_1} + V_{12} + V_{23} + V_{34} \end{aligned}$$

where $V_{ij} = V_j - V_i$. The passage matrix P between these two bases can be thus written as

$$\mathbf{P} = \begin{pmatrix} 0 & 0 & 0 \\ 1 & 0 & 0 \\ 1 & 1 & 0 \\ 1 & 1 & 1 \end{pmatrix} \tag{2.89}$$

The Hamiltonian $\mathcal{H}$ is then obtained by the Legendre transformation $\mathcal{H} = \hbar \sum_{j=1}^{3} \dot{\varphi}_j n_j - \mathcal{L}$ and thus writes

$$\mathcal{H} = \frac{(2e)^2}{2} \boldsymbol{n}^T \left(\mathbf{P}^T \mathbf{C} \mathbf{P}\right)^{-1} \boldsymbol{n} + U \tag{2.90}$$

This Hamiltonian can be expressed in the so-called charge basis $|n_1, n_2, n_3\rangle$, $\forall n_1, n_2, n_3 \in \mathbb{Z}^3$, noting that

$$\cos\varphi_j |n_1, n_2, n_3\rangle = \frac{1}{2}\left(|n_1 + \delta_{j1}, n_2 + \delta_{j2}, n_3 + \delta_{j3}\rangle + |n_1 - \delta_{j1}, n_2 - \delta_{j2}, n_3 - \delta_{j3}\rangle\right) \tag{2.91}$$

In this basis the operator $\frac{(2e)^2}{2}\boldsymbol{n}^T\left(\mathbf{P}^T\mathbf{C}\mathbf{P}\right)^{-1}\boldsymbol{n}$ is diagonal while the operator U is sparse. The precision of the eigenvalues and eigenstates depends on the truncation of the n_j bases. With $n_k = -10\ldots 10$, we would need 21^3 coefficients just to describe the wavefunction and another $\left(21^3\right)^2$ to describe the Hamiltonian matrix. Thanks to the the sparsity of the Hamiltonian operator, the number of nonzero entries in this matrix is only $21^3 \times (1 + 4 \times 2)$. This resolution in charge space is computationally feasible both to store and diagonalize matrices efficiently.

2.2.3.4 Pseudo-Hamiltonian

Following the full diagonalization of the Hamiltonian, we obtain the spectrum of the flux qubit by subtracting the energy of the first excited state $|1\rangle$ from the energy of the ground state $|0\rangle$. It can be shown that close to $\Phi/\varphi_0 = \pi$, the system behaves as a two level system and the spectrum can be fully described by two parameters:

- The value of the persistent current I_p, already discussed previously.
- The so-called flux qubit gap, denoted as Δ, which corresponds to the tunneling term between the two potential minima.

The value of the gap can be directly measured by the transition energy at half a flux quantum $\Phi/\varphi_0 = \pi$. This point is known as the *optimal point* of the flux qubit due to its immunity at first order in flux noise, as will be explained in later sections. In the vicinity of the optimal point, the Hamiltonian of the system can be written using perturbation theory as

$$\begin{aligned}\mathcal{H} &= \mathcal{H}_0 - \alpha E_J \partial_\Phi \left(\cos\left(2\pi\frac{\Phi}{\Phi_0} - \sum_{j=1}^{3}\varphi_j\right)\right)_{\Phi=\Phi_0/2} \cdot \left(\Phi - \frac{\Phi_0}{2}\right) \\ &= \mathcal{H}_0 + \frac{1}{\varphi_0}\left[\underbrace{\alpha E_J \sin(\varphi_\alpha)}_{\hat{I}\cdot\varphi_0}\left(\Phi - \frac{\Phi_0}{2}\right)\right] = \mathcal{H}_0 + \hat{I}\cdot\left(\Phi - \frac{\Phi_0}{2}\right)\end{aligned} \tag{2.92}$$

When the current operator is projected on the eigenstates $|0\rangle$, $|1\rangle$ of $\mathcal{H}_0$ we get

$$\begin{aligned}\langle 0|\,\hat{I}\,|0\rangle = 0 \ , \ \langle 0|\,\hat{I}\,|1\rangle = I_p \\ \langle 1|\,\hat{I}\,|0\rangle = I_p \ , \ \langle 1|\,\hat{I}\,|1\rangle = 0\end{aligned} \tag{2.93}$$

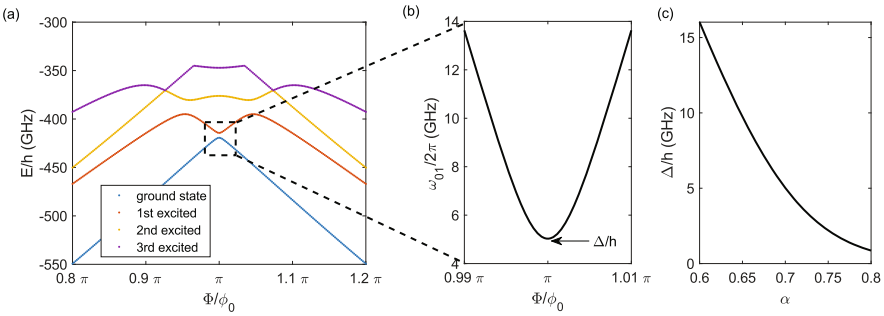

Fig. 2.15 Flux qubit energy levels. (**a**) Calculated eigenenergies of the flux qubit circuit versus applied magnetic field. The calculations were performed using a 3-junction qubit with $E_J/h = 350$ GHz, $E_C/h = 5$ GHz and $\alpha = 0.7$. (**b**) Calculated qubit spectroscopy in the close vicinity of $\Phi/\varphi_0 = \pi$. At precisely $\Phi/\varphi_0 = \pi$, the transition energy of the qubit is minimal and equal to the gap Δ. (**c**) Qubit minimal frequency (Δ/h) versus α parameter

Therefore, the Hamiltonian of the system can be written in this basis as

$$\boxed{\mathcal{H}_{\text{eff}} = \frac{\hbar}{2}\left[\Delta\sigma_z + \varepsilon\sigma_x\right]} \tag{2.94}$$

where $\varepsilon = \frac{2I_p}{\hbar}(\Phi - \pi\varphi_0)$. The frequency of the flux qubit is thus given by

$$\omega_{01} = \sqrt{\Delta^2 + \varepsilon^2} \tag{2.95}$$

2.2.3.5 Improving Flux Qubit Design

As shown in Fig. 2.15b, the flux qubit resonance frequency is strongly dependent on the value of the applied magnetic flux. Away from $\Phi/\varphi_0 = \pi$, the coherence of the qubit will be compromised by the presence of flux noise. We will study this question more in details in Sect. 2.4.2.4. The only point where one can expect to have long coherence time is the so-called "optimal point" where the qubit frequency is minimal and thus immune to flux noise at first order. At that point the flux qubit transition energy is equal to the flux qubit gap Δ. The flux qubit gap is strongly dependent on the design parameters of the junctions (E_J, E_C) and on the value of α as shown in Fig. 2.15c. This means that an extreme precision in the fabrication of the qubit is needed if one wishes to control the value of the gap [18].

Tunable Flux Qubits

It is possible to create a tunable flux qubit by replacing one of the junction by a SQUID as is done for the split Cooper pair box in Sect. 2.2.2.2. This approach brings necessarily a new channel of decoherence to the qubit [19] which should be controlled properly, for instance by using SQUIDS with large assymetry [20].

Fluxonium

The fluxonium has been developed in 2009 at Yale University [21]. The main idea of this design consists of reducing the flux sensitivity of the qubit by increasing the number of junctions intersecting the loop of the circuit. As shown in Sect. 2.2.3.1, the introduction of a large number of junctions (typically ~ 50) reduces dramatically the value of the persistent current flowing in the loop of the qubit and thus its magnetic dipole moment. In addition, this qubit is immune to charge noise and exhibits a large increase of its relaxation time at $\Phi/\varphi_0 = \pi$ due to destructive interference of quasiparticles [22]. A large enhancement of the coherence time compared to flux qubits was indeed observed [23]. The main limitations of this design are its rather low transition frequencies (in the range of few hundreds of MHz at optimal point), which require dynamical initialization of the qubit. Moreover, the tiny magnetic moment of the fluxonium reduces its ability to be easily coupled to other qubits, resonators and/or quantum devices.

Capacitively-Shunted Flux Qubits

In this design developed at MIT in 2016, the flux qubit is connected to a big capacitance which reduces strongly the persistent current and anharmonicity of the qubit [24, 25]. In a recent work [25], a capacitively shunted flux qubit embedded into a three-dimensional cavity has shown relaxation times up to $T_1 \sim 90\ \mu s$ and Ramsey decoherence time of $T_{2R} \sim 18\ \mu s$.

2.3 Coupling Qubits and Resonators

In this chapter, we will describe succinctly how qubits and resonators can be coupled together in order to establish the main ingredients required for the functioning of a quantum processor. Our objective is not to give a comprehensive overview of the field of circuit-QED but rather to focus on the basic principles of qubit readout and manipulation.

2.3.1 Coupling a Qubit with a Resonator

Charge and flux qubit can be coupled to a resonator by capacitive or inductive coupling. The value of this coupling depends on the electric/magnetic zero-field fluctuations of the resonator at the qubit position and on the electric or magnetic moment of the qubit.

2.3.1.1 Transmon Embedded in a Three-Dimensional Cavity

For instance, let us consider a transmon embedded into a three-dimensional rectangular cavity shown in Fig. 2.16. The transmon is composed of two pads separated by a short distance d and connected by a wire intersected by a single Josephson junction (see [9]). The zero-field fluctuations of the electric field in the

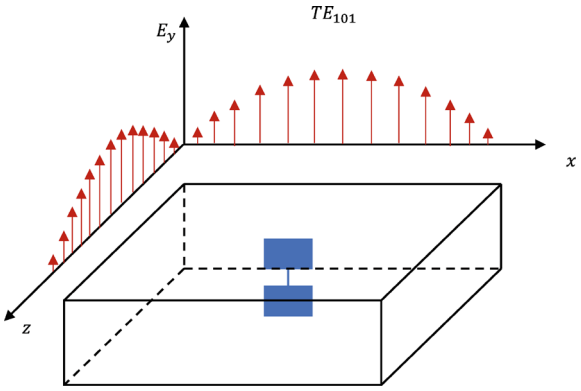

Fig. 2.16 Transmon qubit embedded into a three dimensional cavity. The qubit is coupled to the electric field E_y of the fundamental mode (TE101) of the cavity

cavity can be easily estimated by integrating the electric field energy density over the whole volume V and thus calculating the energy stored in the cavity

$$\int_V \varepsilon_0 \delta E_0^2(x, y, z)\, dx\, dy\, dz = \frac{\hbar\omega}{2} \tag{2.96}$$

The coupling between the fundamental cavity mode (TE101 represented in Fig. 2.16) and a qubit situated in the center of the cavity is thus given by

$$\hbar g = ed\delta E_0 = \frac{ed}{2}\sqrt{\frac{\hbar\omega}{2\varepsilon_0 V}} \tag{2.97}$$

This simple back-of-the-envelope estimation can be applied for instance to the cavity-qubit system described in [9] where $d = 100\,\mu\text{m}$, $\omega = 8\,\text{GHz}$ and $V = 3\,\text{cm}^3$ and gives $\frac{g}{2\pi} = 125\,\text{MHz}$, which is very close to the coupling constant extracted experimentally from spectroscopic measurement in the same publication.

2.3.1.2 Flux Qubit Coupled Inductively to a Lumped Element Resonator

Another interesting example consists of a flux qubit coupled inductively to a lumped element resonator as shown in Fig. 2.17. The flux qubit is placed at a distance d from the resonator inductance and is coupled to the current fluctuations of the resonator.

Assuming the current is flowing in an infinitely-thin wire, it is possible to calculate analytically the magnetic field in the vicinity of the qubit using Biot Savart law. Namely,

$$\delta B_0 = \mu_0 \frac{\delta I_0}{2\pi r} \tag{2.98}$$

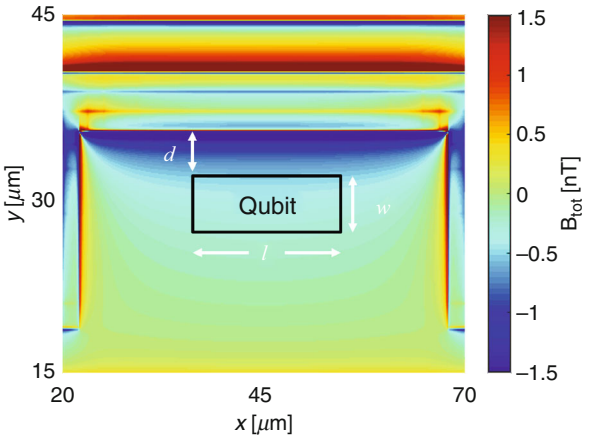

Fig. 2.17 Flux qubit coupled inductively to a resonator. The magnetic field is calculated from the current flowing in the resonator using an electromagnetic simulator (Sonnet)

The coupling between the resonator and the qubit is obtained by integrating the magnetic field threading the loop of the qubit. Using Eq. (2.94),

$$\hbar g = I_p \int \delta B_0 dS = M I_P \delta I_0 \tag{2.99}$$

where $M = \frac{\mu_0 l}{2\pi} \ln\left(1 + \frac{w}{d}\right)$ is the mutual inductance and δI_0 are the current quantum fluctuations of the resonator (see Eq. (2.58)). This simple back-of-the-envelope estimation can be applied for instance to the system shown in Fig. 2.17 where $d = 1\ \mu\text{m}$, $w = l = 3\ \mu\text{m}$, $I_p = 300\ \text{nA}$ and $\delta I_0 = 40\ \text{nA}$. We obtain $M = 0.8\ \text{pH}$ and $\frac{g}{2\pi} = 15\ \text{MHz}$.

The mutual inductance can be increased further by connecting galvanically the qubit loop to the resonator. In this configuration, the mutual inductance per unit length M/l reaches approximately $3\,\text{pH}/\mu\text{m}$ for wires of cross section $200 \times 40\,\text{nm}^2$ and thus the coupling can reach $\frac{g}{2\pi} = 170\,\text{MHz}$, assuming $I_p = 300\ \text{nA}$ and $\delta I_0 = 40\ \text{nA}$.

2.3.1.3 Qubit Readout by Dispersive Shift

The Hamiltonian of a qubit coupled to a resonator can be written as

$$\mathcal{H} = \hbar\omega_r a^+ a + \frac{1}{2}\hbar\omega_{01}\sigma_z + V \tag{2.100}$$

where $V = \hbar g\left(\sigma^+ + \sigma^-\right)\left(a + a^+\right)$, g being the coupling calculated in the sections herein above. The expansion of this product of operators involves four terms. The terms proportional to $\sigma^+ a$ and $\sigma^- a^+$correspond to transitions from lower (resp. upper) level of the qubit together with the annihilation (resp. creation) of a photon in the resonator. The two other terms $\sigma^+ a^+$ and $\sigma^- a$ correspond to transitions from lower (resp. upper) level of the qubit together with creation (resp. annihilation) of a photon in the resonator. When the frequency of the qubit and the resonator

are sufficiently close, these terms correspond to highly non-resonant processes. Neglecting these anti-resonant terms is a standard approximation in Quantum Electrodynamics called Rotative Wave Approximation (RWA).

For simplicity, we will make this approximation in the following and consider

$$V = \hbar g \left(\sigma^+ a + \sigma^- a^+\right) \tag{2.101}$$

Within this approximation, the qubit and the resonator frequencies are assumed to be relatively close. When the qubit and the resonator are detuned and the coupling is sufficiently small ($g \ll |\omega_{01} - \omega_r|$), one can transform the Hamiltonian using a unitary transformation $U = e^S$, where S is an anti-hermitian operator chosen to satisfy (see Sect. 2.5.2.3)

$$\left[S, \hbar\omega_r a^+ a + \frac{1}{2}\hbar\omega_{01}\sigma_z\right] = -V \tag{2.102}$$

It is straightforward to show that this condition is satisfied by choosing

$$S = \frac{g}{\omega_{01} - \omega_r}\left(\sigma^+ a - \sigma^- a^+\right) \tag{2.103}$$

Using this transformation, the Hamiltonian can be described in a perturbative approach (see Sect. 2.5.2.3) as

$$\widetilde{H} \simeq \hbar\omega_r a^+ a + \frac{1}{2}\hbar\omega_{01}\sigma_z + \frac{g^2}{(\omega_{01} - \omega_r)}\sigma_z\left(a^+ a + \frac{1}{2}\right) \tag{2.104}$$

This last term corresponds to a Lamb shift effect. The frequency of the qubit is shifted by the presence of photons in the cavity. This will have important consequences on the qubit coherence as will be seen in Sect. 2.4.2.5. The same term viewed from the resonator perspective corresponds to a change of the resonator frequency depending on the state of the qubit. When the qubit is in the excited state, the resonator frequency is offset from ω_r by

$$\boxed{\delta_1\omega_r = \frac{g^2}{(\omega_{01} - \omega_r)}} \tag{2.105}$$

When the qubit is in the ground state, the resonator frequency is offset from its bare frequency ω_r by an opposite value

$$\boxed{\delta_0\omega_r = -\frac{g^2}{(\omega_{01} - \omega_r)}} \tag{2.106}$$

This frequency shift is usually called dispersive shift and allows the detection of the qubit state by looking at the frequency shift of its coupled resonator. In order to be able to detect it easily, this shift should be comparable with the resonator linewidth.

2.3.2 Single Qubit Gates

2.3.2.1 Driving a Qubit by a Classical Drive

Arbitrary single-qubit rotations can be realized by applying a classical drive for a certain time duration. The Hamiltonian of the system can be written as

$$\mathcal{H} = \hbar\frac{\omega_{01}}{2}\sigma_z + \hbar\Omega\sigma_x \cos\left(\omega_{mw}t + \varphi\right) \tag{2.107}$$

where ω_{01} is the qubit frequency, ω_{mw} is the drive frequency, φ the phase of the drive and Ω is the Rabi frequency and is proportional to the drive amplitude. The equations of motion which describe the qubit evolution taking into account decoherence are derived in Appendix 2.5.1.7.

Under unitary transformation $U = \exp\left(\boldsymbol{i}\sigma_z\frac{\omega_{mw}}{2}t\right)$, the Hamiltonian becomes (see Appendix 2.5.2.1)

$$\begin{aligned}\widetilde{\mathcal{H}} = \hbar\frac{\delta}{2}\sigma_z + \hbar\frac{\Omega}{2}\left(\sigma^+\exp\left(\boldsymbol{i}\omega_{mw}t\right) + \sigma^-\exp\left(-\boldsymbol{i}\omega_{mw}t\right)\right)\left(\exp\left(\boldsymbol{i}\left(\omega_{mw}t + \varphi\right)\right)\right.\\ \left.+\exp\left(-\boldsymbol{i}\left(\omega_{mw}t + \varphi\right)\right)\right)\end{aligned} \tag{2.108}$$

where $\delta = \omega_{01} - \omega_{mw}$ is the detuning between the drive and the qubit frequency. Neglecting the terms rotating at $2\omega_{mw}$ (Rotative Wave Approximation), one obtains a time-independent effective Hamiltonian

$$\widetilde{\mathcal{H}} = \hbar\frac{\delta}{2}\sigma_z + \hbar\frac{\Omega}{2}\left(\sigma^+\exp\left(-\boldsymbol{i}\varphi\right) + \sigma^-\exp\left(+\boldsymbol{i}\varphi\right)\right) \tag{2.109}$$

For $\delta = 0$, the evolution under such Hamiltonian is relatively simple

$$U(\tau) = \begin{pmatrix} \cos\left(\frac{\Omega\tau}{2}\right) & -\boldsymbol{i}\sin\left(\frac{\Omega\tau}{2}\right)e^{-\boldsymbol{i}\varphi} \\ -\boldsymbol{i}\sin\left(\frac{\Omega\tau}{2}\right)e^{\boldsymbol{i}\varphi} & \cos\left(\frac{\Omega\tau}{2}\right) \end{pmatrix} \tag{2.110}$$

In particular a $\pi/2$ pulse ($\Omega\tau = \pi/2$) will take a qubit in the ground state $|0\rangle$ to an equal superposition of ground and excited:

$$\begin{aligned}|0\rangle &\rightarrow \frac{1}{\sqrt{2}}\left(|0\rangle - \boldsymbol{i}e^{-\boldsymbol{i}\varphi}|1\rangle\right)\\ |1\rangle &\rightarrow \frac{1}{\sqrt{2}}\left(-\boldsymbol{i}e^{\boldsymbol{i}\varphi}|0\rangle + |1\rangle\right)\end{aligned}$$

A π pulse ($\Omega\tau = \pi$) will take a qubit in the ground state $|0\rangle$ to the excited state and vice versa

$$|0\rangle \rightarrow -ie^{-i\varphi}|1\rangle$$
$$|1\rangle \rightarrow -ie^{i\varphi}|0\rangle$$

2.3.2.2 Driving a Qubit via a Resonator Port

It is possible to drive the qubits that are positioned inside of a resonator by using one of the resonator ports. In the following we calculate the Rabi frequency of a flux qubit coupled inductively to a $\lambda/2$ transmission line resonator (see Sect. 2.1.5.5). According to (2.60)

$$\hat{I}(x) = \frac{1}{\sqrt{Z_0}} \sum_n \left(f_{\rightarrow}(\omega_n, x)\, A^{\rightarrow}_{L,n} + f_{\leftarrow}(\omega_n, x)\, A^{\leftarrow}_{R,n} \right) + \text{H.c.} \tag{2.111}$$

Let us assume that we drive a monochromatic wave ($\omega_n = \omega_{01}$) from the left such that $A^{\leftarrow}_{R,n} = 0, \forall n$. The resulting Rabi frequency (see Eq. (2.94)) is

$$\Omega^{\rightarrow} = \frac{2MI_p}{\hbar}\sqrt{\frac{1}{Z_0}}\left| f_{\rightarrow}(\omega_{01}, x)\, A^{\rightarrow}_{L}(\omega_{01}) \right| \tag{2.112}$$

Since $\left|A^{\rightarrow}_{L}(\omega_{01})\right|^2 = \langle P \rangle / 2$ (see (2.22)), we get

$$\boxed{(\hbar\Omega^{\rightarrow})^2 / \langle P \rangle = \frac{(2MI_p)^2}{2Z_0} |f_{\rightarrow}(\omega_{01}, x)|^2} \tag{2.113}$$

The same can be done for a monochromatic drive from the right, assuming $A^{\rightarrow}_{L,n} = 0, \forall n$. Thus we get

$$\boxed{(\hbar\Omega^{\leftarrow})^2 / \langle P \rangle = \frac{(2MI_p)^2}{2Z_0} |f_{\leftarrow}(\omega_{01}, x)|^2} \tag{2.114}$$

2.3.3 Two-Qubit Gates

2.3.3.1 Coupling Two Qubits by Fixed Coupling

One of the simplest two-qubit coupling scheme consists of coupling neighboring qubits with a static coupling. These neighboring qubits are naturally coupled by dipole-dipole interaction. The coupling is mainly electric (capacitive) for charge qubits and magnetic (inductive) for flux qubits. It is possible to increase the coupling strength by using an intermediate lumped element as shown in Fig. 2.18.

In the following, we will illustrate how this coupling is established between two transmon qubits. This kind of coupling has already been described for resonators in Sect. 2.1.2.3.

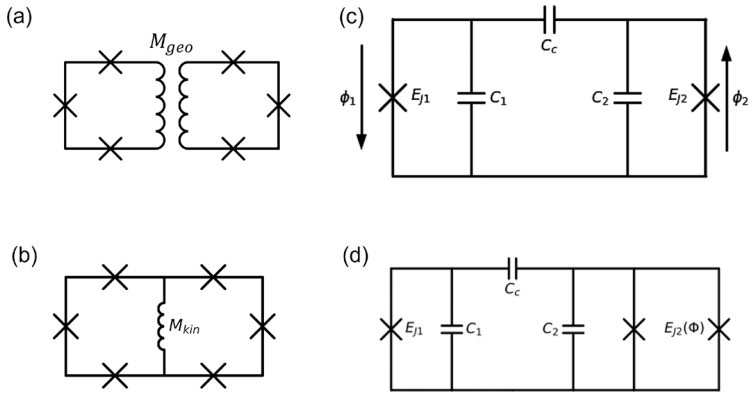

Fig. 2.18 Different coupling schemes (**a**) Inductive coupling by geometric mutual inductance M_{geo} between two flux qubits. (**b**) Inductive coupling by sharing a lumped element inductance M_{kin} between the qubits. (**c**) Capacitive coupling by sharing a coupling capacitance C_c between two transmon qubits. (**d**) Controllable coupling by tuning the frequency of a tunable transmon via a DC flux

The Lagrangian of two capacitively coupled transmon qubits (shown in Fig. 2.18c) is given by

$$\mathcal{L} = T - V = \left[\frac{1}{2}C_1\dot{\Phi_1}^2 + \frac{1}{2}C_2\dot{\Phi_2}^2 + \frac{1}{2}C_C\left(\dot{\Phi_1} - \dot{\Phi_2}\right)^2\right] + \left[E_{J_1}\cos\left(\frac{\Phi_1}{\varphi_0}\right) + E_{J_2}\cos\left(\frac{\Phi_2}{\varphi_0}\right)\right]$$

The conjugate momenta are defined by

$$Q_1 = \frac{\partial\mathcal{L}}{\partial\dot{\Phi_1}} = C_1\dot{\Phi_1} + C_C\left(\dot{\Phi_1} - \dot{\Phi_2}\right)$$

$$Q_2 = \frac{\partial\mathcal{L}}{\partial\dot{\Phi_2}} = C_2\dot{\Phi_2} - C_C\left(\dot{\Phi_1} - \dot{\Phi_2}\right)$$

We then obtain the Hamiltonian of the system $H = Q_1\dot{\Phi_1} + Q_2\dot{\Phi_2} - \mathcal{L}$ and decompose it into three elements $H = H_1 + H_2 + V$ such that

$$H_1 = \frac{1}{2}\beta\left(C_2 + C_C\right)Q_1^2 - E_{J_1}\cos\left(\frac{\Phi_1}{\varphi_0}\right) \sim \frac{1}{2}\hbar\omega_1\sigma_1^z$$

$$H_2 = \frac{1}{2}\beta\left(C_1 + C_C\right)Q_1^2 - E_{J_2}\cos\left(\frac{\Phi_2}{\varphi_0}\right) \sim \frac{1}{2}\hbar\omega_2\sigma_2^z$$

$$\boxed{V = \beta C_C Q_1 Q_2 \sim \hbar g\left(\sigma_1^- - \sigma_1^+\right)\left(\sigma_2^+ - \sigma_2^-\right)} \tag{2.115}$$

where $\beta = \frac{1}{C_C C_1 + C_C C_2 + C_2 C_1}$, $\omega_{1/2} = \frac{\sqrt{E_{J_{1/2}} \beta (C_{2/1} + C_C)}}{\varphi_0}$ and

$$g = -\frac{1}{2} \beta C_C \sqrt{\omega_1 \omega_2} \sqrt{(C_C + C_1)(C_C + C_2)}. \tag{2.116}$$

The product expansion of V involves four terms. Performing a Rotating Wave Approximation (RWA) allows us to neglect the two non-resonant terms, and obtain

$$V = \hbar g \left(\sigma_1^+ \sigma_2^- + \sigma_1^- \sigma_2^+ \right). \tag{2.117}$$

2.3.3.2 iSWAP Gate

This interaction allows us to perform a two qubit gate when the detuning $\delta = \omega_1 - \omega_2$ between the two qubits is smaller than g ($\delta << g$). In order to better understand this point, we calculate the time-evolution matrix of the system

$$U(t) = \begin{pmatrix} 1 & 0 & 0 & 0 \\ 0 & \cos[g_e t] - \boldsymbol{i} \frac{\delta}{g_e} \sin[g_e t] & \boldsymbol{i} \frac{2g}{g_e} \sin[g_e t] & 0 \\ 0 & \boldsymbol{i} \frac{2g}{g_e} \sin[g_e t] & \cos[g_e t] + \boldsymbol{i} \frac{\delta}{g_e} \sin[g_e t] & 0 \\ 0 & 0 & 0 & 1 \end{pmatrix} \tag{2.118}$$

where $g_e = \sqrt{4g^2 + \delta^2}$ is the effective swapping frequency. We can see that in the case where $\delta >> g$, the off-diagonal matrix elements goes to 0, and no energy transfer can be made between the two qubits. However, in the case where $\delta = 0$, the qubits can exchange their excitations. For example, after time $t = \frac{\pi}{4g}$ we can perform the so-called iSWAP gate defined by

$$iSWAP = \begin{pmatrix} 1 & 0 & 0 & 0 \\ 0 & 0 & \boldsymbol{i} & 0 \\ 0 & \boldsymbol{i} & 0 & 0 \\ 0 & 0 & 0 & 1 \end{pmatrix}$$

In practice, it is difficult and undesirable to fabricate qubits at the same resonance frequency. Indeed, if all qubits were at the same frequency, it would be impossible to control them separately. In Fig. 2.18d, we present a slightly different realization of a two-qubit gate dealing with this challenge. The frequency of one qubit is tuned to match the resonance frequency of the other by adding a SQUID which acts as a tunable-inductor (see Sect. 2.2.2.2). The inductance of a SQUID $L_J(\Phi)$ depends on the magnetic flux Φ threading its loop. Therefore, applying DC pulses on the SQUID enables one to tune δ such that $\delta << g$ turning the gate 'on' and 'off' on demand. On one hand, this realization surely shows advantages in controlled gate operations. On the other hand, adding the SQUID to the qubit introduces some decoherence.

2.3.3.3 Controlled-Z Gate

The transmon weak anharmonicity allows implementing a so-called controlled-Z gate. Contrary to the iSWAP gate, this gate is not based on tuning the qubit transition frequencies into resonance with each other but rather exploits the third energy level of the transmon (see Sect. 2.2.2.3).

The idea of this gate consists of tuning the qubits to a point where the $|1, 1\rangle$ and $|0, 2\rangle$ are degenerate in the absence of coupling [12]. In presence of the coupling, the two states can exchange energy and it is thus possible by letting them evolve freely during an appropriate delay time to transfer state $|1, 1\rangle$ to $-|1, 1\rangle$ and thus have

$$CZ = \begin{pmatrix} 1 & 0 & 0 & 0 \\ 0 & 1 & 0 & 0 \\ 0 & 0 & 1 & 0 \\ 0 & 0 & 0 & -1 \end{pmatrix} \tag{2.119}$$

2.3.3.4 Tunable Coupling Mediated by a Resonator or a Qubit

Two-qubit gates can also be mediated by an intermediate resonator [26, 27] or by a coupling qubit [12]. In Fig. 2.19, we present a possible implementation of such a scheme. Two transmon qubits are coupled by capacitors C_{c1} and C_{c2} to a common coupler whose frequency is controllable by a flux Φ threading a SQUID loop. In addition, the two transmons are coupled directly by capacitor C_{12}.

As we will see in the following, the advantage of this implementation is the ability to control directly the coupling between the two qubits without having to detune them out of their optimal working point. In addition, one can also cancel completely the direct coupling due to C_{12} by adjusting the frequency of the coupler and it is thus possible to operate properly each qubit independently with good fidelity.

In the following, we will derive the Hamiltonian of two qubits while considering the coupler as an intermediate resonator. Assuming Rotating Wave Approximation, we have

$$\mathcal{H} = \frac{\hbar\omega_1}{2}\sigma_1^z + \frac{\hbar\omega_2}{2}\sigma_2^z + \hbar\omega_r a^\dagger a + \hbar g_1\left(\sigma_1^+ a + \sigma_1^- a^\dagger\right) + \hbar g_2\left(\sigma_2^+ a + \sigma_2^- a^\dagger\right) \tag{2.120}$$

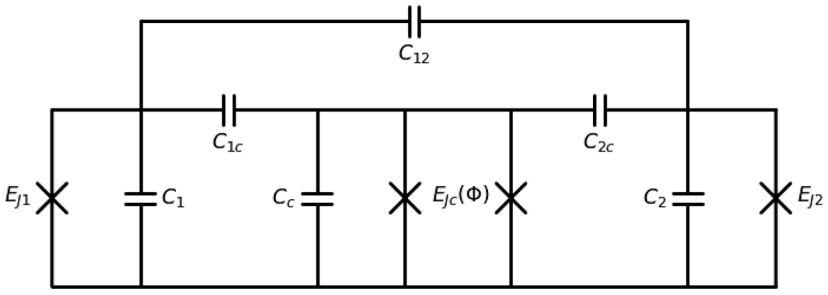

Fig. 2.19 Mediated Coupling between two transmon qubits. The two qubits are coupled to a coupler element by capacitors C_{c1} and C_{c2}. The frequency of the coupler is controllable by a flux threading the SQUID loop

In the case where the detunings are much larger than the coupling constants, it is possible to trace out the degree of freedom of the intermediate coupler by using a Schrieffer Wolff transformation (see Sect. 2.5.2.3)

$$S = \frac{g_1}{\omega_1 - \omega_r}\left(\sigma_1^+ a - \sigma_1^- a^+\right) + \frac{g_2}{\omega_2 - \omega_r}\left(\sigma_2^+ a - \sigma_2^- a^+\right)$$

and get an effective Hamiltonian

$$H_{\text{eff}} = \frac{\hbar\omega_1}{2}\sigma_1^z + \frac{\hbar\omega_2}{2}\sigma_2^z + \hbar\left(\omega_r + \chi_1\sigma_1^z + \chi_2\sigma_2^z\right)a^\dagger a + \hbar g_{\text{eff}}\left(\sigma_1^+\sigma_2^- + \sigma_1^-\sigma_2^+\right) \tag{2.121}$$

where $\chi_i = \frac{g_i^2}{\delta_i}$, and an effective interaction

$$\boxed{g_e = \frac{g_1 g_2\left(\delta_1 + \delta_2\right)}{2\delta_1\delta_2}} \tag{2.122}$$

By tuning properly the frequency of the coupler at $\omega_r = \frac{\omega_1+\omega_2}{2} + \frac{g_1 g_2}{2g_{12}}\left[1 \pm \sqrt{1 + \left(\frac{g_{12}(\omega_1-\omega_2)}{g_1 g_2}\right)^2}\right]$, it is possible to cancel the small direct coupling term $V_{12} = \hbar g_{12}\left(\sigma_1^+\sigma_2^- + \sigma_1^-\sigma_2^+\right)$ between the qubits. This choice enables to operate single qubit gates with maximum fidelity. When the coupling between two qubits is needed, the coupler frequency is changed quickly by applying DC current on a flux line in the vicinity of the SQUID shown in Fig. 2.19.

2.3.3.5 Microwave Dynamic Coupling

A different approach is to apply a resonant microwave-drive on a qubit in order to dress this qubit in effective resonance with another. The advantage of this coupling scheme is that one can turn on and off the coupling by the application of a microwave tone. In this section, we will try to explain briefly this strategy in a simple case. We consider two qubits which are coupled directly by coupling constant g. One applies a time-dependent resonant Rabi drive on qubit 1. The driven Hamiltonian writes

$$\mathcal{H} = \hbar\frac{\omega_1}{2}\sigma_1^z + \frac{\hbar\omega_2}{2}\sigma_2^z + \hbar g\sigma_1^x\sigma_2^x + \hbar\Omega\sigma_1^x\cos\left(\omega_1 t\right) \tag{2.123}$$

Under unitary transformation $U_1 = \exp\left(i\frac{\omega_1}{2}(\sigma_1^z + \sigma_2^z)t\right)$, the Hamiltonian becomes (see Appendix 2.5.2.1) after rotating wave approximation

$$\widetilde{\mathcal{H}_1} = \hbar\frac{\delta}{2}\sigma_2^z + \hbar\frac{\Omega}{2}\sigma_1^x + \hbar g\left(\sigma_1^+\sigma_2^- + \sigma_1^-\sigma_2^+\right) \tag{2.124}$$

The eigenstates associated to eigenvalues $\pm\Omega/2$ of $\hbar\Omega/2\sigma_1^x$ are

$$|+\rangle = \frac{|0\rangle + |1\rangle}{\sqrt{2}}$$
$$|-\rangle = \frac{|0\rangle - |1\rangle}{\sqrt{2}}$$

The splitting of these two levels is at the origin of Rabi oscillations. The operators can be rewritten in the basis of $|\mp\rangle$ as

$$\sigma_1^+ = |1\rangle\langle 0| = (|+\rangle - |-\rangle)\,(\langle +| + \langle -|)\,/2$$
$$\sigma_1^- = |0\rangle\langle 1| = (|+\rangle + |-\rangle)\,(\langle +| - \langle -|)\,/2$$

Under this basis change, the above operators can be replaced by

$$\sigma_1^{\pm} \to \left(\sigma_1^z \mp \boldsymbol{i}\sigma_1^y\right)/2$$
$$\sigma_1^x \to \sigma_1^z$$

In this basis $\widetilde{\mathcal{H}}$ can be written as

$$\begin{aligned}\widetilde{\mathcal{H}}_1 &= H_0 + V\\ H_0 &= \hbar\Omega\frac{\sigma_1^z}{2} + \hbar\delta\frac{\sigma_2^z}{2}\\ V &= \hbar g\left(\frac{\sigma_1^z - \boldsymbol{i}\sigma_1^y}{2}\sigma_2^- + \frac{\sigma_1^z + \boldsymbol{i}\sigma_1^y}{2}\sigma_2^+\right)\end{aligned} \tag{2.125}$$

The expression of operators $\sigma_1^-, \sigma_1^+, \sigma_2^-, \sigma_2^+$ under unitary transformation $U_2 = \exp\left(\boldsymbol{i}(\frac{\Omega}{2}\sigma_z^1 + \frac{\delta}{2}\sigma_z^2)t\right)$ can be easily estimated using Baker Campbell Hausdorff formula (see Sect. 2.5.2.2)

$$\sigma_1^+ \to \sigma_1^+ e^{+\boldsymbol{i}\Omega t}$$
$$\sigma_1^- \to \sigma_1^- e^{-\boldsymbol{i}\Omega t}$$
$$\sigma_2^+ \to \sigma_2^+ e^{+\boldsymbol{i}\delta t}$$
$$\sigma_2^- \to \sigma_2^- e^{-\boldsymbol{i}\delta t}$$

Therefore under this transformation, the Hamiltonian becomes

$$\widetilde{\mathcal{H}}_2 = U_2 V U_2^+ = \hbar g \left(\frac{\sigma_1^z + \sigma_1^- e^{-i\Omega t} - \sigma_1^+ e^{+i\Omega t}}{2} \sigma_2^- e^{-i\delta t} + \frac{\sigma_1^z + \sigma_1^+ e^{+i\Omega t} - \sigma_1^- e^{-i\Omega t}}{2} \sigma_2^+ e^{+i\delta t} \right) \tag{2.126}$$

If $\Omega \approx \delta$, only two terms of this Hamiltonian will be time independent giving rise to an effective Hamiltonian

$$H_{\Omega=\delta} = -\frac{\hbar g}{2} \left(\sigma_1^+ \sigma_2^- + \sigma_1^- \sigma_2^+ \right)$$

One of the main advantage of the dynamical coupling techniques is that they can be directly generalized to large registers with minimal extra hardware and control lines. Along these lines, several protocols have been proposed and realized in recent years. For instance, one can apply a resonant Rabi frequency drive on both qubits at the same time as suggested in Ref. [28, 29] or one can even drive one qubit at the resonant frequency of the other qubit [30], inducing dynamics in the latter across the connecting resonator. These techniques (FLICFORQ, Cross Resonance,...) are frequently used in recent experiments.

2.4 Relaxation and Decoherence

One of the main limitations of quantum computers is related to the uncontrolled influence of the environment. An efficient quantum processor should have a scalable register of qubits that is easy to initialize, readout and manipulate but that is at the same time well-protected from variations of the parameters of its environment. These variations of parameters can cause uncontrolled changes in the qubits state, reducing our ability to perform well-defined operations. This process is called decoherence and is characterized by two distinct rates. The depolarization rate Γ_1 corresponds to an energy exchange with the environment. The pure dephasing rate Γ_φ is associated to low-frequency noise, which affects the Larmor frequency of the qubit without energy exchange. The two processes of relaxation and pure dephasing combine to the so-called decoherence rate[3]

$$\boxed{\Gamma_2 = \frac{1}{2}\Gamma_1 + \Gamma_\varphi}$$

[3] Note that the definition of Γ_2 as a sum of rates is only strictly valid when the noise spectra are Lorentzians centers around zero frequency and decay functions are exponential.

2.4.1 Relaxation

2.4.1.1 Fermi Golden Rule

The relaxation rate Γ_1 corresponds to energy exchange between the qubit and its environment. In principle, this rate is the sum of excitation and relaxation rates of the qubit with its environment

$$\Gamma_1 = \Gamma_{1\to 0}^{rel} + \Gamma_{0\to 1}^{exc} \tag{2.127}$$

Within the assumption that the qubit is weakly coupled to its environment, $\Gamma_{1\to 0}^{rel}$ and $\Gamma_{0\to 1}^{exc}$ can be estimated using Fermi Golden Rule

$$\Gamma_{1\to 0}^{rel} = \frac{2\pi}{\hbar^2} \sum_{n,m} \rho_{nn} \left|\langle 1, m \left| V_{int} \right| 0, n\rangle\right|^2 \delta\left(\omega_m - \omega_n - \omega_{01}\right) \tag{2.128}$$

$$\Gamma_{0\to 1}^{exc} = \frac{2\pi}{\hbar^2} \sum_{n,m} \rho_{nn} \left|\langle 0, m \left| V_{int} \right| 1, n\rangle\right|^2 \delta\left(\omega_m - \omega_n + \omega_{01}\right) \tag{2.129}$$

where ρ_{nn} are the diagonal elements of the density operator of the surrounding bath. There are no quantum correlations in the bath and thus all non-diagonal elements of the density operator are equal to zero.

2.4.1.2 Link Between the Fermi Golden Rule and the Power Spectrum of a Bath Operator

In the following we assume that the coupling of the qubit to the environment can be written as $V_{int} = \lambda \sigma_x F$ where F is an arbitrary operator acting on the environment degrees of freedom. The correlations of operator $F(t)$ are given by

$$\begin{aligned}
\langle F\left(t\right) F\left(0\right)\rangle &= \mathrm{Tr}\left(\rho F\left(t\right) F\left(0\right)\right) = \sum_n \rho_{nn} \langle n \left| F(t) F(0) \right| n\rangle \\
&= \sum_{n,m} \rho_{nn} \langle n \left| F(t) \right| m\rangle \langle m \left| F(0) \right| n\rangle \\
&= \sum_{n,m} \rho_{nn} \left\langle n \left| e^{\boldsymbol{i} Ht/\hbar} F(0) e^{-\boldsymbol{i} Ht/\hbar} \right| m \right\rangle \langle m \left| F(0) \right| n\rangle \\
&= \sum_{n,m} \rho_{nn} e^{\boldsymbol{i}\left(\omega_n - \omega_m\right)t} \left|\langle m \left| F \right| n\rangle\right|^2
\end{aligned}$$

According to Wiener-Khintchine theorem, the power spectrum $S_F\left(\omega\right)$ is related to the correlations by

$$\begin{aligned}
S_F\left(\omega\right) &= \frac{1}{2\pi} \int_{t\in\mathbb{R}} \langle F\left(t\right) F\left(0\right)\rangle e^{\boldsymbol{i}\omega t} \\
&= \sum_{n,m} \rho_{nn} \left|\langle m \left| F \right| n\rangle\right|^2 \delta\left(\omega_m - \omega_n - \omega\right)
\end{aligned}$$

It is thus possible to express the relaxations rates as a function of the power spectrum of operator F

$$\boxed{\Gamma_{1\to 0}^{rel} = \frac{2\pi}{\hbar^2} |\lambda|^2 S_F(\omega_{01})} \tag{2.130}$$

$$\boxed{\Gamma_{0\to 1}^{exc} = \frac{2\pi}{\hbar^2} |\lambda|^2 S_F(-\omega_{01})} \tag{2.131}$$

In superconducting qubits, the temperature of the bath is usually much smaller than the qubit frequency and thus $\Gamma_{0\to 1}^{exc}$ is exponentially suppressed by a Boltzmann factor $\exp[-\hbar\omega_{01}/k_B T]$.

2.4.1.3 Wigner Weisskopf Theory of Relaxation

In the following, we will consider a qubit coupled to a bath of harmonic oscillators within the Wigner-Weisskopf theory of relaxation. The system is described by the following Hamiltonian

$$\mathcal{H} = \hbar\frac{\omega_{01}}{2}\sigma_z + \sum \hbar\omega_k a_k^+ a_k + \hbar\sigma_x \sum g_k(a_k^+ + a_k) \tag{2.132}$$

We write the Heisenberg equations for a_k and σ_z operators as

$$\dot{a}_k = \frac{i}{\hbar}\left[\mathcal{H}, a_k\right] = -i\omega_k a_k - i g_k \sigma_x$$

$$\dot{a}_k^+ = \frac{i}{\hbar}\left[\mathcal{H}, a_k^+\right] = i\omega_k a_k^+ + i g_k \sigma_x$$

$$\dot{\sigma}_z = \frac{i}{\hbar}\left[\mathcal{H}, \sigma_z\right] = 2\sigma_y \sum g_k(a_k^+ + a_k)$$

We assume that at time $t = 0$, the spin is in its excited state and thus $\langle\sigma_z(t=0)\rangle = 1$ and the bath is empty $\forall k \ \langle a_k(t=0)\rangle = 0$. At time $t = +\infty$, the spin is de-excited and $\forall k \ \left\langle a_k^+(t=+\infty)\right\rangle = 0$. Using these boundary conditions, we can easily integrate the first two equations

$$a_k(t) = -i g_k \int_0^t e^{-i\omega_k(t-t')}\sigma_x(t')\,dt'$$

$$a_k^+(t) = -i g_k \int_t^{+\infty} e^{i\omega_k(t-t')}\sigma_x(t')\,dt'$$

By replacing these expression we get

$$\dot{\sigma}_z(t) = -2\boldsymbol{i}\sum g_k^2\left[\sigma_y(t)\left(\int_t^{+\infty} e^{\boldsymbol{i}\omega_k(t-t')}\sigma_x(t')\,dt'\right)\right.$$
$$\left.+\sigma_y(t)\left(\int_0^t e^{-\boldsymbol{i}\omega_k(t-t')}\sigma_x(t')\,dt'\right)\right] \tag{2.133}$$

We can simplify this expression assuming $g_k = g\ \forall k$ (Markovian approximation) and using

$$\Delta\omega\sum e^{\pm\boldsymbol{i}\omega_k t} \simeq \int_0^{+\infty} e^{\pm\boldsymbol{i}\omega t}\,d\omega = [\pi\delta(t) \pm \boldsymbol{i}\,P\frac{1}{t}]$$

where P denotes the Cauchy principal value and $\Delta\omega$ the constant spacing between different values of ω_k. Moreover,

$$\int_0^t \sigma_x(t')\delta(t-t')\,dt' = \int_t^{+\infty} \sigma_x(t')\delta(t-t')\,dt' = \sigma_x(t)/2 \tag{2.134}$$

Thus, we get

$$\dot{\sigma}_z(t) = -2\pi g^2\frac{1}{\Delta\omega}\sigma_z(t) = -\Gamma_1\sigma_z(t) \tag{2.135}$$

This last expression enables us to extract an expression of the relaxation rate Γ_1 of the qubit

$$\boxed{\Gamma_1 = \frac{2\pi g^2}{\Delta\omega}}$$

2.4.1.4 Relaxation of a Qubit Coupled to a Single Mode Resonator: Purcell Effect

In the following, we will consider a qubit embedded into a single mode resonator. For simplicity, we consider a system described by the so-called Jaynes-Cummings Hamiltonian

$$\mathcal{H} = \hbar\frac{\omega_{01}}{2}\sigma_z + \hbar\omega_r a^+a + \hbar g(\sigma^+a + \sigma^-a^+) \tag{2.136}$$

We assume the resonator is coupled to the external environment with a Lindblad jump operator $L = \sqrt{\kappa}a$. The presence of a dissipation channel for the resonator opens an effective dissipation for the qubit due to the presence of the coupling g. This effect is called Purcell effect and should be carefully taken into account when designing a circuit-QED experiment.

When the qubit and the resonator are sufficiently detuned $g \ll |\omega_{01} - \omega_r|$, the Hamiltonian can be replaced by an effective Hamiltonian using a Schrieffer-Wolff transformation $U = e^S$ where $S = \frac{g}{\omega_{01}-\omega_r}\left(\sigma^+ a - \sigma^- a^+\right)$ (see Chap. 2.5.2.4). This transformation enables us to estimate the Purcell effect. Indeed, the equations of motion of the density operator in this new frame $\widetilde{\rho}$ should include Lindblad jump operators expressed in the same frame

$$\widetilde{L} = e^S L e^{-S} \tag{2.137}$$

Using Baker Campbell Hausdorff formula (see Sect. 2.5.2.2), we get

$$\widetilde{L} \sim L + [S, L] = \sqrt{\kappa} a + \frac{g}{\omega_{01} - \omega_r}\sqrt{\kappa}\sigma^- \tag{2.138}$$

We can now write the equation of motion of operator σ_z using Sect. 2.5.1.6

$$\dot{\sigma}_z(t) = -\frac{g^2\kappa}{(\omega_{01} - \omega_r)^2}(\sigma_z + \mathbb{1}) \tag{2.139}$$

and thus we can extract the Purcell relaxation rate Γ_1^P

$$\boxed{\Gamma_1^P = \frac{g^2\kappa}{(\omega_{01} - \omega_r)^2}} \tag{2.140}$$

2.4.1.5 Purcell Rate in a Transmission Line Resonator

In the following, we will consider as an illustration the Hamiltonian of a flux qubit coupled inductively to a transmission line resonator

$$H = \hbar\omega_{01}\frac{\sigma_z}{2} + M I_p \hat{I}(x)\,\sigma_x \tag{2.141}$$

We denote as Γ_1^P the Purcell relaxation rate of the qubit due to its coupling with the resonator. Using Eqs. (2.130) and 2.131, we have

$$\Gamma_1^P = \frac{2\pi}{\hbar^2} M^2 I_p^2 \left[S_I(\omega_{01}) + S_I(-\omega_{01})\right]$$

We recall that according to Eq. (2.50), $I(x, \omega)$ can be expressed as a function of the propagation wave amplitudes $A_L^{\rightarrow}(\omega)$ and $A_R^{\leftarrow}(\omega)$ in the incoming lines as

$$I(x, \omega) = \frac{1}{\sqrt{Z_0}}\left(f_{\rightarrow}(x, \omega) A_L^{\rightarrow}(\omega) + f_{\leftarrow}(x, \omega) A_R^{\leftarrow}(\omega)\right) \tag{2.142}$$

Due to the independence of signals $A_L^{\rightarrow}(\omega)$ and $A_R^{\leftarrow}(\omega)$, we have

$$S_I(\omega) = \frac{1}{Z_0}\left(|f_{\rightarrow}(\omega, x)|^2 S_{A_L^{\rightarrow}}(\omega) + |f_{\leftarrow}(\omega, x)|^2 S_{A_R^{\leftarrow}}(\omega)\right) \tag{2.143}$$

Using $A_k^{\rightarrow} = \sqrt{\frac{c}{2\Lambda}\hbar\omega_k}\, a_k^{\rightarrow}$ (see Sect. 2.1.4.4) we calculate

$$\begin{aligned} S_{A_L^{\rightarrow}}(\omega) &\equiv \frac{1}{2\pi}\int_{t\in\mathbb{R}} \left\langle A_L^{\rightarrow}(t)\, A_L^{\rightarrow}(0)\right\rangle e^{i\omega t} \\ &= \frac{1}{2\pi}\sum_{n\geq 0}\left(\frac{c}{2\Lambda}\hbar\omega_n\right)\int_{t\in\mathbb{R}}\left(\left\langle \left(a_{L,n}^{\rightarrow}\right)^{\dagger} a_{L,n}^{\rightarrow}\right\rangle e^{+i\omega_n t}\right. \\ &\quad \left. + \left\langle a_{L,n}^{\rightarrow}\left(a_{L,n}^{\rightarrow}\right)^{\dagger}\right\rangle e^{-i\omega_n t}\right) e^{i\omega t} \\ &= \sum_{n\geq 0}\left(\frac{c}{2\Lambda}\hbar\omega_n\right)\left(\left\langle \left(a_{L,n}^{\rightarrow}\right)^{\dagger} a_{L,n}^{\rightarrow}\right\rangle \delta(\omega_n+\omega) + \left\langle a_{L,n}^{\rightarrow}\left(a_{L,n}^{\rightarrow}\right)^{\dagger}\right\rangle \delta(\omega_n-\omega)\right) \end{aligned}$$

By replacing the discrete sum $\sum_{n\geq 0}$ by its equivalent integral $\int_{d\omega\in\mathbb{R}_+}\eta(\omega)$, we get

$$\begin{aligned} S_{A_L^{\rightarrow}}(\omega) &= \int_{d\omega'\in\mathbb{R}_+}\frac{\hbar\omega'}{4\pi}\left(\left\langle a^{\dagger}a\right\rangle\delta(\omega'+\omega) + \left\langle aa^{\dagger}\right\rangle\delta(-\omega'+\omega)\right) \\ &= \begin{cases} \frac{\hbar\omega}{4\pi}\left\langle aa^{\dagger}\right\rangle & \omega > 0 \\ \frac{\hbar\omega}{4\pi}\left\langle a^{\dagger}a\right\rangle & \omega < 0 \end{cases} \end{aligned} \tag{2.144}$$

By considering that the photon bath is thermalized at a given temperature T,

$$S_{A_L^{\rightarrow}}(\omega) = \begin{cases} \frac{\hbar\omega}{4\pi}\frac{1}{1-e^{-\beta\hbar\omega}} & \omega > 0 \\ \frac{\hbar\omega}{4\pi}\frac{e^{-\beta\hbar\omega}}{1-e^{-\beta\hbar\omega}} & \omega < 0 \end{cases} \tag{2.145}$$

where $\beta = \frac{1}{k_B T}$. Finally, the Purcell decay rate writes

$$\Gamma_1^P = \left(\frac{MI_p}{\hbar}\right)^2 \frac{\hbar\omega_{01}\coth\left(\frac{\hbar\omega_{01}}{2k_BT}\right)\left(|f_{\rightarrow}(\omega_{01},x)|^2 + |f_{\leftarrow}(\omega_{01},x)|^2\right)}{2Z_0} \tag{2.146}$$

which we separate into two parts

$$\Gamma_1^P = \Gamma_1^{\rightarrow} + \Gamma_1^{\leftarrow} \tag{2.147}$$

where

$$\Gamma_1^{\rightarrow/\leftarrow} = \left(\frac{MI_p}{\hbar}\right)^2 \frac{\hbar\omega_{01}}{2Z_0}\left|f_{\rightarrow/\leftarrow}(\omega_{01},x)\right|^2 \coth\left(\frac{\beta\hbar\omega_{01}}{2}\right) \tag{2.148}$$

2.4.1.6 Calculating the Purcell Rate from Rabi Frequency

Considering Eqs. 2.148, (2.113), and (2.114), we establish a relationship valid at zero temperature

$$\boxed{\Gamma_1^{\rightarrow/\leftarrow}(0\,K) = \frac{\hbar\omega_{01}\left(\Omega^{\rightarrow/\leftarrow}\right)^2}{4\langle P\rangle}} \tag{2.149}$$

We thus get

$$\Gamma_1^P(0\,K) = \frac{\hbar\omega_{01}\left[(\Omega^{\rightarrow})^2 + (\Omega^{\leftarrow})^2\right]}{4\langle P\rangle} \tag{2.150}$$

The advantage of this formula is that it gives directly the Purcell rate via the measurement of the Rabi frequency for a given average power $\langle P\rangle$ with a precision limited by the uncertainty on $\langle P\rangle$, which is typically ± 1 dB.

2.4.1.7 Dielectric Losses

The typical relaxation times of superconducting qubits have been largely improved by the introduction of three dimensional cavity, which reduce the impact of dielectric losses in the circuit [9, 17, 25]. Various works have tried to reduce these losses in order to increase the fidelity of the qubit [10, 11, 18] while keeping a 2D scalable architecture. This can be done by reducing the interface defects between the metal and the substrate [11].

Dielectric losses take place in the capacitors and can be modeled by a small resistor of resistance R in series with each capacitor. The value of R is determined by the loss tangent of the dielectric material separating each island and is given by

$$RC\omega_{01} = \tan\delta \tag{2.151}$$

As a result, the noise voltage generated by the (lossy) capacitor is given by

$$S_{\delta V}(\omega_{01}) + S_{\delta V}(-\omega_{01}) = \frac{R\hbar\omega_{01}}{\pi}\coth\left(\frac{\beta\hbar\omega_{01}}{2}\right) \approx \frac{\hbar\omega_{01}R}{\pi} \tag{2.152}$$

To calculate the relaxation rate of a qubit, one must determine the transverse term $\sigma_{x/y}$ in the Hamiltonian introduced by a small perturbation δV. For instance, one can calculate the relaxation of a transmon due to dielectric losses in the substrate. The variation of the charge across the capacitor C due to δV is given by $\delta Q = -C\delta V$. At first order in δV, this modifies the kinetic term of the Hamiltonian by $dK = \delta Q\,\hat{V}$. Using Eq. (2.130), we get

$$\Gamma_1^{\text{diel}} = \frac{2\pi}{\hbar^2}C^2\left|\left\langle 1\left|\hat{V}\right|0\right\rangle\right|^2 S_{\delta V}(\omega_{01}) \tag{2.153}$$

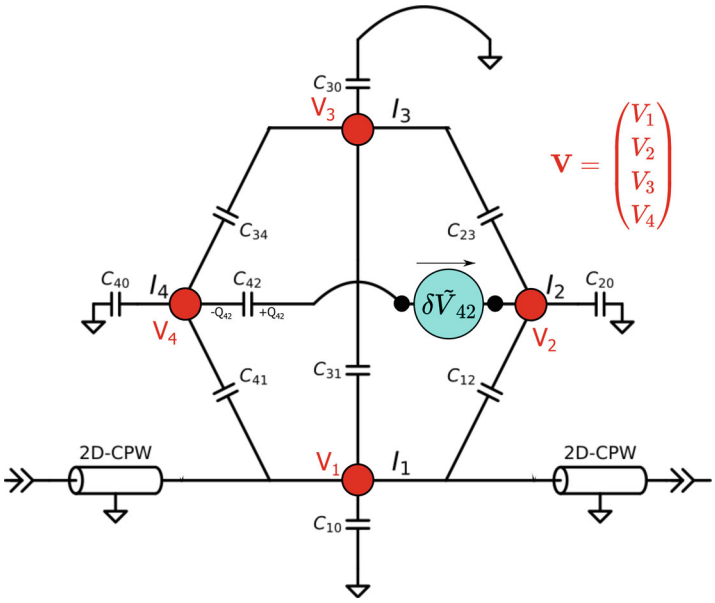

Fig. 2.20 Dielectric losses of a flux qubit. An external bias δV_{ij}(cyan) is applied. Here we show the example of $(i, j) = (4, 2)$, where we write $Q_{42} = C_{42}\left(V_4 - \left(V_2 + \tilde{V}_{42}\right)\right)$

which gives

$$\boxed{\Gamma_1^{\text{diel}} = \frac{16}{\hbar} E_C \left|\langle 1 \left|\hat{n}\right| 0\rangle\right|^2 \tan\delta} \tag{2.154}$$

where $E_C = \frac{e^2}{2C}$, $\hat{n} = \frac{C\hat{V}}{2e}$. For a typical transmon on sapphire substrate $\left(\tan\delta \sim 10^{-6}\right)$ with $E_J/\hbar = 20$ GHz and $E_C/\hbar = 200$ MHz, the value of the transition matrix element is $\left|\langle 1 \left|\hat{n}\right| 0\rangle\right|^2 \sim 1.7$ and thus $\Gamma_1^{\text{diel}} \sim 5$ kHz.

In the following, we will calculate the dielectric losses for a flux qubit with four junctions. As we can see in Fig. 2.20, the variation of charge across the capacitor C_{42} due to δV_{42} is given by

$$\delta Q_{42} = -C_{42}\delta V_{42} \tag{2.155}$$

At first order in δV_{ij}, this modifies the kinetic term by

$$\begin{aligned} dK_{42} &= \delta Q_{42}\left(V_2 - V_4\right) \\ &= -C_{42}\delta V_{42}\mathbf{V}^T \begin{pmatrix} 0 \\ 1 \\ 0 \\ -1 \end{pmatrix} \end{aligned}$$

Let us recall that $\mathbf{P}$ from (2.89) is the 4×3 transfer matrix from the junction coordinates to the island phases such that $\mathbf{V} = \mathbf{P}\dot{\mathbf{\Phi}} = \mathbf{P}\left(\mathbf{P}^T\mathbf{C}\mathbf{P}\right)^{-1}\boldsymbol{Q}$ (up to a constant). Injecting and generalizing to all other indices ij, we can write the total perturbation of the Hamiltonian to all perturbations δV_{ij}.

$$\begin{aligned} dH &= \sum_{i \neq j} \left(-dK_{ij}\right) \\ &= \sum_{i \neq j} C_{ij}\delta V_{ij}\boldsymbol{Q}^T\left(\mathbf{P}^T\mathbf{C}\mathbf{P}\right)^{-1}\mathbf{P}^T\left(\mathbf{e}_j - \mathbf{e}_i\right) \end{aligned}$$

where $\mathbf{e}_i$ is the sparse column vector with 1 only at position i.

Let us define the 3×3 real symmetrical matrix comprised of the quantum overlaps of the charge operators

$$\mathbf{Q^2} = \left(\langle 1|Q_i|0\rangle\langle 0|Q_j|1\rangle, \forall i, j \in \{1,2,3\}\right) \tag{2.156}$$

Seeing that dH is linear in the $\boldsymbol{Q}$ operators we can write dH under the form

$$\begin{aligned} dH &= \delta V_{ij} \cdot \left(\boldsymbol{Q}^T\boldsymbol{L_{ij}}\right) \\ \boldsymbol{L_{ij}} &= C_{ij}\left(\mathbf{P}^T\mathbf{C}\mathbf{P}\right)^{-1}\mathbf{P}^T\left(\mathbf{e}_i - \mathbf{e}_j\right) \end{aligned}$$

Subsequently, the loss rate due to δV_{ij} writes

$$\begin{aligned} \Gamma_{ij} &= 2\pi\frac{\left[S_{\delta V_{ij}}(\omega_{01}) + S_{\delta V_{ij}}(-\omega_{01})\right]\boldsymbol{L_{ij}}^T\mathbf{Q^2}\boldsymbol{L_{ij}}}{\hbar^2} \\ &= (2\omega_{01}R/\hbar)\,\mathrm{Tr}\left(\boldsymbol{L_{ij}}\boldsymbol{L_{ij}}^T\mathbf{Q^2}\right) \\ &= \left(2\tan\delta_{ij}/\hbar C_{ij}\right)\mathrm{Tr}\left(\boldsymbol{L_{ij}}\boldsymbol{L_{ij}}^T\mathbf{Q^2}\right) \end{aligned}$$

where we replace the expression of R in the last equality according to (2.151). We get

$$\Gamma_{ij} = \frac{2}{\hbar}\mathrm{Tr}\left(\left(\mathbf{P}^T\mathbf{C}\mathbf{P}\right)^{-1}\left[\mathbf{P}^T\left(\mathbf{e}_i - \mathbf{e}_j\right)C_{ij}\tan\delta_{ij}\left(\mathbf{e}_i - \mathbf{e}_j\right)^T\mathbf{P}\right]\left(\mathbf{P}^T\mathbf{C}\mathbf{P}\right)^{-1}\mathbf{Q^2}\right) \tag{2.157}$$

After summation over all island pairs i, j in $[\cdot]$, we get

$$\boxed{\Gamma_1^{\mathrm{diel}} = \frac{2}{\hbar}\mathrm{Tr}\left(\left(\mathbf{P}^T\mathbf{C}\mathbf{P}\right)^{-1}\left(\mathbf{P}^T\mathbf{P}\right)\left(\mathbf{P}^T\mathbf{C}\mathbf{P}\right)^{-1}\mathbf{Q^2}\right)} \tag{2.158}$$

where $= \sum_{ij} \left(\mathbf{e}_i - \mathbf{e}_j\right) C_{ij} \tan\delta_{ij} \left(\mathbf{e}_i - \mathbf{e}_j\right)^T$ is the capacitance matrix *weighted* by the $\tan\delta$ of individual capacitive elements (we recover, for the *unweighted* expression, the usual capacitance matrix $\mathbf{C} = \sum_{ij} \left(\mathbf{e}_i - \mathbf{e}_j\right) C_{ij} \left(\mathbf{e}_i - \mathbf{e}_j\right)^T$). In the case where $\tan\delta$ is homogeneous over all the different capacitances , we get

$$\boxed{\Gamma_1^{\text{diel}} = \frac{2}{\hbar} \text{Tr}\left(\left(\mathbf{P}^T \mathbf{C} \mathbf{P}\right)^{-1} \mathbf{Q^2}\right) \tan\delta} \tag{2.159}$$

2.4.2 Pure Dephasing

2.4.2.1 General Framework for the Pure Dephasing of a Qubit

In an ideal system, the decoherence rate Γ_2 is limited by the energy relaxation rate of the qubit and is given by $\Gamma_2 = \Gamma_1/2$. In practice, the decoherence rate of a qubit may be much larger than this theoretical limit due to pure dephasing. The pure dephasing rate Γ_φ is associated to low-frequency noise, which affects the Larmor frequency of the qubit without energy exchange.

In order to estimate this effect more precisely, we write the Heisenberg equations of a qubit in free precession in the frame rotating at the average Larmor frequency of the qubit $\langle\omega_{01}\rangle$

$$\begin{aligned}
\frac{d\sigma^+}{dt} &= \boldsymbol{i}\,\delta(t)\sigma^+ \\
\frac{d\sigma^-}{dt} &= -\boldsymbol{i}\,\delta(t)\sigma^- \\
\frac{d\sigma_z}{dt} &= 0
\end{aligned}$$

where $\delta(t) = \omega_{01}(t) - \langle\omega_{01}\rangle$. These differential equations are decoupled and can be solved straightforwardly

$$\begin{aligned}
\sigma^+(t) &= e^{\boldsymbol{i}\int_0^t \delta(t)\,dt}\sigma^+(0) \\
\sigma^-(t) &= e^{-\boldsymbol{i}\int_0^t \delta(t)\,dt}\sigma^-(0)
\end{aligned}$$

The phase $\varphi(t) = \int_0^t \delta(t)\,dt$ depends on small fluctuations $\lambda(t)$ which slightly modify the qubit Hamiltonian. At first order, $\delta(t)$ is given by $\delta(t) = \frac{\partial\omega_{01}}{\partial\lambda}\lambda(t)$. The pure dephasing rate of the system corresponds to the decay of the expectation value $\left\langle\sigma^\pm(t)\right\rangle$ and is given by

$$\left\langle\sigma^\pm(t)\right\rangle = \left\langle e^{\pm i\varphi(t)}\right\rangle \sigma^+(0) \tag{2.160}$$

If the fluctuations $\delta\lambda(t)$ are small enough, they can be considered as a random variable with Gaussian distribution [31]. Thus, using Isserlis theorem, we get

$$f_R(t) = \left\langle e^{\pm i\varphi(t)} \right\rangle \simeq e^{-1/2\langle\varphi^2(t)\rangle} \tag{2.161}$$

The expectation value of $\langle\sigma^{\pm}(t)\rangle$ will therefore decay according to

$$f_R(t) = e^{-1/2\left(\frac{\partial\omega_{01}}{\partial\lambda}\right)^2\left\langle\left(\int_0^t \lambda(t')dt'\right)^2\right\rangle} \tag{2.162}$$

We can write

$$\left\langle\left(\int_0^t \lambda(t')dt'\right)^2\right\rangle = \int_{t\in\mathbb{R}}\int_{u\in\mathbb{R}} dt'\,du\,\left\langle\lambda(t'-u)\lambda(0)\right\rangle H(t')H(u') \tag{2.163}$$

Where $H(u)$ is the boxcar function such that $H(u) = 1$ if $0 \leq u \leq t$ and zero elsewhere. Using Wiener Khinchine theorem to express the correlations as a function of the power spectrum $S_\lambda(\omega)$

$$\langle\lambda(t)\,\lambda(0)\rangle = \int d\omega e^{-i\omega t} S_\lambda(\omega) \tag{2.164}$$

Noting that

$$\int_{u\in\mathbb{R}} du\; H(u)e^{\pm i\omega u} = t\,\mathrm{sinc}(\frac{\omega t}{2}) \tag{2.165}$$

we get

$$\boxed{f_R(t) = \exp\left(-\frac{t^2}{2}\left(\frac{\partial\omega_{01}}{\partial\lambda}\right)^2 \int_{-\infty}^{\infty} d\omega\, S_\lambda(\omega)\,\mathrm{sinc}^2(\frac{\omega t}{2})\right)} \tag{2.166}$$

2.4.2.2 Dynamical Decoupling

Experimentally, the pure dephasing rate of a qubit can be estimated by the so-called *Ramsey sequence*, where two identical $\pi/2$ pulses are played consecutively after a time delay t. It is possible to dynamically decouple the noise responsible for this dephasing by playing a more complex set of pulses. The most popular technique to achieve this is called *Hahn Echo technique* and consists of playing a π-pulse in between the two $\pi/2$ pulses. This π pulse inverses the time evolution and therefore cancels the contribution to dephasing of low frequency noise.

In a Hahn echo sequence, the first $\pi/2$-pulse puts the state of the qubit in a coherent superposition state. During the time t_1, the qubit performs a free evolution and accumulates phase $\varphi_1(t_1) = \int_0^{t_1}\delta_1(t')dt'$. The π—pulse flips the time evolution

of the qubit such that during the time t_2 it acquires an opposite phase $\varphi_2(t_2) = -\int_{t_1}^{t_1+t_2} \delta_2(t')dt'$. Assuming that the environment is static during the free evolution, the phase accumulated is completely canceled if $t_1 = t_2 = t/2$.

In practice the noise is not static and the decoherence rate of the qubit—corresponding to the decay $f_E(t) = \langle \sigma^{\pm}(t) \rangle$—is given by

$$f_E(t) = \left\langle e^{\pm i(\delta_1 - \delta_2)} \right\rangle \approx \exp\left(-1/2 \left\langle \delta_1^2 + \delta_2^2 - \delta_1\delta_2 - \delta_2\delta_1 \right\rangle \right) \tag{2.167}$$

After a calculation similar to the one performed in previous section [31], one can show that the expectation value of $\langle \sigma^{\pm}(t) \rangle$ will decay according to

$$\boxed{f_E(t) = \exp\left(-\frac{t^2}{2} \left(\frac{\partial \omega_{01}}{\partial \lambda} \right)^2 \int_{-\infty}^{\infty} d\omega \, S_\lambda(\omega) \sin^2(\frac{\omega t}{4}) \operatorname{sinc}^2(\frac{\omega t}{4}) \right)} \tag{2.168}$$

White Spectrum

If the power spectrum is white ($S_\lambda(\omega) = S_\lambda(\omega = 0)$) , it is possible to calculate analytically the pure dephasing rate. Indeed,

$$\int_{-\infty}^{\infty} d\omega \operatorname{sinc}^2(\frac{\omega t}{2}) = \int_{-\infty}^{\infty} d\omega \sin^2(\frac{\omega t}{4}) \operatorname{sinc}^2(\frac{\omega t}{4}) = \frac{2\pi}{t} \tag{2.169}$$

The dynamical decoupling is therefore not effective for white noise. The Ramsey and Echo sequence give the same *exponential* decay, namely

$$\Gamma_{\varphi R} = \Gamma_{\varphi E} = \pi \left(\frac{\partial \omega_{01}}{\partial \lambda} \right)^2 S_\lambda(\omega = 0) \tag{2.170}$$

This result can be generalized if the power spectrum is regular at $\omega = 0$ on a frequency scale $|\omega| \leq 1/t$. Indeed,

$$\int_{-\infty}^{\infty} d\omega \, S_\lambda(\omega) \operatorname{sinc}^2(\frac{\omega t}{2}) \simeq S_\lambda(0) \int_{-\infty}^{\infty} d\omega \operatorname{sinc}^2(\frac{\omega t}{2}) \tag{2.171}$$

1/f Spectrum

Here we assume that the power spectrum follows a 1/f law in a wide range of frequencies limited by an infrared cutoff ω_{IR} and an ultraviolet cutoff ω_c

$$S_\lambda(\omega) = \frac{A}{|\omega|}, \quad \omega_{IR} \leq |\omega| \leq \omega_c \tag{2.172}$$

The infrared cutoff is usually determined by the total length of the measurement protocol (typically 1Hz) and the ultraviolet cutoff is typically in the range of a few MHz. Using

$$\int_{\omega_{IR}}^{\infty} \frac{d\omega}{|\omega|} \mathrm{sinc}^2(\frac{\omega t}{2}) \simeq 2\ln\left(\frac{1}{\omega_{IR} t}\right) \tag{2.173}$$

$$\int_{-\infty}^{\infty} \frac{d\omega}{|\omega|} \sin^2(\frac{\omega t}{4}) \mathrm{sinc}^2(\frac{\omega t}{4}) = 2\ln(2) \tag{2.174}$$

we get a *Gaussian* decay for both Ramsey and Echo pure dephasing with

$$\Gamma_{\varphi R} = \sqrt{A}\left(\frac{\partial \omega_{01}}{\partial \lambda}\right)\sqrt{\ln\left(\frac{1}{\omega_{IR} t}\right)} \tag{2.175}$$

$$\Gamma_{\varphi E} = \sqrt{A}\left(\frac{\partial \omega_{01}}{\partial \lambda}\right)\sqrt{\ln(2)} \tag{2.176}$$

In particular, $\sqrt{\ln\left(\frac{1}{\omega_{IR} t}\right)} \sim 3.7$ and $\Gamma_{\varphi R}/\Gamma_{\varphi E} \sim 4.5$ for typical cutoff frequencies. This limited echo efficiency is due to the high frequency tail of 1/f noise.

2.4.2.3 Charge Noise in a Transmon Qubit

An important source of pure dephasing for qubits is noise on the charge of each island of the qubit. This noise is due to microscopic charged fluctuators that can be either trapped electrons or ions in defects of the material that move between two or several metastable positions. These charge fluctuators are partly located in the substrate and partly on the oxide layers covering the electrodes of the device.

The charge noise power spectrum follows approximately a 1/f behavior up to frequencies of approximately 1 MHz

$$S_Q(\omega) = \frac{A_Q}{|\omega|} \tag{2.177}$$

The typical amplitude A_Q depends on the parameters of the experiment (temperature, size of the island, screening by other electrodes). A typical value is $\sqrt{A_Q} \sim 10^{-3} e$ where $e = 1.6 \times 10^{-19}$ C is the electron charge.

Several qubit design have been used to reduce the influence of this noise. In particular, a transmon with a large ratio E_J/E_C will have a small charge dispersion (see Fig. 2.11b), which will reduce the dephasing due to charge noise.

Taking a charge qubit with $\omega_{01}/2\pi = 5$ GHz and $E_J/E_C = 10$, we see in Fig. 2.11b that $\frac{\partial\omega_{01}}{\partial n_g} \sim 10^7$ rad/s. Thus, using Eq. (2.176), we get $\Gamma_{\varphi E}^{\text{charge}} \sim 10$ kHz. If we increase further E_J/E_C to the transmon regime, it is possible to cancel almost completely the charge dispersion, reducing therefore the contribution of charge noise to decoherence.

2.4.2.4 Dephasing of a Flux Qubit Away from its Optimal Point

Flux noise is also an important source of dephasing for qubits which posses a superconducting loop, such as flux qubits. The origin of this noise is most likely due to microscopic spins in the vicinity of the qubit which generate a magnetic noise threading the loop of the qubit. The flux noise power spectrum follows approximately a 1/f behavior up to high frequencies [16]

$$S_\Phi(\omega) = \frac{A_\Phi}{|\omega|} \tag{2.178}$$

The typical value of the flux noise amplitude is $\sqrt{A_\Phi} \sim 10^{-6}\Phi_0$ where $\Phi_0 = 2 \times 10^{-15}$ Wb is the magnetic flux quantum.

To illustrate our discussion, we will consider in the following a flux qubit away from its optimal point. As already mentioned in Sect. 2.2.3.5, the high magnetic moment of the flux qubit make its frequency very sensitive to flux

$$\frac{\partial\omega_{01}}{\partial\Phi} = \frac{\partial\varepsilon}{\partial\Phi}.\frac{\partial\omega_{01}}{\partial\varepsilon} = \left(\frac{2I_p}{\hbar}\right)^2 \frac{(\Phi - \Phi_0/2)}{\omega_{01}} \tag{2.179}$$

Taking a flux qubit with $\omega_{01}/2\pi = 5$ GHz, $I_p = 300$ nA, $\Phi - \Phi_0/2 = 50\,\mu\Phi_0$, and using Eq. (2.176), we get $\Gamma_{\varphi E}^{\text{flux}} \sim 170$ kHz.

2.4.2.5 Calculating the Dephasing Rate Due to Photon Noise

Stochastic fluctuations in the number of photons in a resonator coupled to a qubit create random dispersive shifts which translates into dephasing. Using Eq. (2.104) , the frequency of the qubit is given by

$$\omega_{01}(t) = \langle\omega_{01}\rangle + 2\chi\,\delta n(t) \tag{2.180}$$

where $\chi = g^2/(\omega_{01} - \omega_r)$ and $\delta n(t) = n(t) - \bar{n}$.

Using Eq. (2.162), one can thus determine the decoherence rate due to photon noise

$$f_R(t) = e^{-1/2(2\chi)^2\left\langle\left(\int_0^t \delta n(t')dt'\right)^2\right\rangle} \tag{2.181}$$

In the following, we compute the correlations $\langle\delta n(\tau)\delta n(0)\rangle$ using quantum regression theorem (see Sect. 2.5.1.8) for thermal and coherent states. More complex photon states in the resonator such as squeezed states can be handled with the same formalism [32].

Thermal Photons

In order to estimate the photon correlations in thermal state of a resonator, we write a set of equations of motion for $\boldsymbol{O} = \left(n(t),\ \mathbb{1}\right)^T$ in presence of Lindblad operators $L_1 = \sqrt{\kappa\,(\bar{n}+1)}a$ and $L_2 = \sqrt{\kappa\bar{n}}a^+$. We obtain coupled differential equations that can be written in the form of

$$\frac{d}{dt}\overrightarrow{O}(t) = G\overrightarrow{O}(t) \tag{2.182}$$

where

$$G = \begin{pmatrix} -\kappa & \kappa\bar{n} \\ 0 & 0 \end{pmatrix} \tag{2.183}$$

The steady-state expectation values are obtained by the null eigenstate of G, defined by $G\langle \boldsymbol{O}\rangle = 0$, leading to $\langle n(t)\rangle_\infty = \bar{n}$. Similarly, we calculate the steady-state expectation value $\langle n^2(t)\rangle_\infty$ using the kernel of the equation of motion for $\hat{n}^2$ and find

$$\langle n^2(t)\rangle_\infty = \bar{n}(2\bar{n}+1) \tag{2.184}$$

To obtain the two-time correlation $\langle n(t+\tau)n(t)\rangle_\infty$, we use the quantum regression theorem (see Sect. 2.5.1.8), namely

$$\frac{d}{d\tau}\begin{pmatrix} \langle n(t+\tau)n(t)\rangle \\ \mathbb{1}\ n(t) \end{pmatrix} = \begin{pmatrix} -\kappa & \kappa\bar{n} \\ 0 & 0 \end{pmatrix}\begin{pmatrix} \langle n(t+\tau)n(t)\rangle \\ \mathbb{1}\ n(t) \end{pmatrix} \tag{2.185}$$

Using the initial conditions $\langle n(t+0)n(t)\rangle_\infty = \bar{n}(2\bar{n}+1)$, we solve the linear differential equation and find

$$\langle n(\tau)n(0)\rangle_\infty = \bar{n}^2 + \left(\bar{n}^2+\bar{n}\right)e^{-\kappa|\tau|} \tag{2.186}$$

Using Wiener Khinchine theorem, we obtain the power spectrum

$$S_n(\omega) = \frac{1}{2\pi}\int_{t\in\mathbb{R}}\langle n(t)n(0)\rangle\, e^{i\omega t} = \frac{\kappa}{\pi}\left(\bar{n}^2+\bar{n}\right)\frac{1}{\kappa^2+\omega^2} \tag{2.187}$$

Typically, the decay rate κ of the resonator is much higher than the decoherence rate of the qubit. The power spectrum $S_n(\omega)$ is almost constant in the range of interest and thus we obtain

$$\boxed{\Gamma_\varphi^{\text{thermal}} = \pi\left(\frac{\partial\omega_{01}}{\partial n}\right)^2 S_n(\omega=0) = \frac{4\chi^2\left(\bar{n}^2+\bar{n}\right)}{\kappa}} \tag{2.188}$$

Coherent States

When the resonator is driven by a classical drive, the resonator is in a coherent state. In the following, we consider the Hamiltonian of an harmonic oscillator in presence of a well-chosen Lindblad operator

$$\mathcal{H} = \hbar\omega_r a^+ a \tag{2.189}$$

$$L = \sqrt{\kappa}\left(a - \alpha e^{i\omega_r t}\right) \tag{2.190}$$

The steady state of this system corresponds to a pure state $\rho(t) = |\psi(t)\rangle\langle\psi(t)|$, where the coherent state $|\psi(t)\rangle = |\alpha e^{i\tilde{\omega}_r t}\rangle$ satisfies $L|\psi(t)\rangle = 0$. Applying the transformation $U = e^{i\omega_r t a^+ a}$ on the Hamiltonian and the Lindblad operator above we obtain

$$\widetilde{\mathcal{H}} = 0 \tag{2.191}$$

$$\widetilde{L} = \sqrt{\kappa}\,(a - \alpha)\, e^{i\omega_r t}. \tag{2.192}$$

In this new frame, we can write the coupled equations of motion for $\boldsymbol{O}$, where $\boldsymbol{O} = \left(n(t),\ a(t),\ a^\dagger(t),\ \mathbb{1}\right)^T$, in the form of $\frac{d}{dt}\overrightarrow{O}(t) = G\overrightarrow{O}(t)$ with

$$G = \begin{pmatrix} -\kappa & \frac{1}{2}\alpha^*\kappa & \frac{1}{2}\alpha\kappa & 0 \\ 0 & -\frac{1}{2}\kappa & 0 & \frac{1}{2}\alpha\kappa \\ 0 & 0 & -\frac{1}{2}\kappa & \frac{1}{2}\alpha^*\kappa \\ 0 & 0 & 0 & 0 \end{pmatrix} \tag{2.193}$$

The steady state solutions result in

$$\langle \boldsymbol{O}\rangle_\infty = \left(|\alpha|^2,\ \alpha,\ \alpha^*,\ 1\right)^T \tag{2.194}$$

In order to find $\langle n(\tau)n(0)\rangle$ we diagonalize the system and plug in the initial conditions in the steady-state solution for $\tau = 0$. Thus, we obtain

$$\langle n(\tau)n(0)\rangle_\infty = |\alpha|^4 + |\alpha|^2\, e^{-\frac{1}{2}\kappa|\tau|} \tag{2.195}$$

Using Wiener Khinchine theorem, we obtain the power spectrum

$$S_n(\omega) = \frac{1}{2\pi}\int_{t\in\mathbb{R}} \langle n(t)n(0)\rangle\, e^{i\omega t} = \frac{\kappa}{2\pi}\bar{n}^2 \frac{1}{(\kappa/2)^2 + \omega^2} \tag{2.196}$$

We obtain therefore the dephasing rate due to photon noise in a coherent-state

$$\boxed{\Gamma_\varphi^{\text{coherent}} = \pi\left(\frac{\partial\omega_{01}}{\partial n}\right)^2 S_n(\omega = 0) = \frac{8\chi^2\bar{n}}{\kappa}} \tag{2.197}$$

2.4.3 Decoherence Under Driven Evolution

The decoherence rate of a driven qubit involves the noise spectral density at its Rabi frequency. To demonstrate this, we will consider in the following a qubit under driven evolution with a drive tuned at the average frequency of the qubit $\langle\omega_{01}\rangle$ assuming that some external fluctuators may modify its instantaneous frequency $\omega_{01}(t)$. The Hamiltonian of the system can be written as

$$\mathcal{H} = \hbar\frac{\omega_{01}(t)}{2}\sigma_z + \hbar\Omega\sigma_x\cos\left(\langle\omega_{01}\rangle\, t\right) \tag{2.198}$$

We introduce a Lindblad jump operator $L_1 = \sqrt{\Gamma_1}\sigma^-$ to describe the relaxation processes. In the following, we assume that $\Gamma_1$is a constant and does not depend on the frequency of the qubit.

We first transform this Hamiltonian with a unitary transformation $U_1(t) = e^{i\frac{\langle\omega_{01}\rangle}{2}\sigma_z t}$ such that the Hamiltonian becomes after rotating wave approximation

$$\widetilde{\mathcal{H}} = \hbar\frac{\delta(t)}{2}\sigma_z + \frac{1}{2}\hbar\Omega\sigma_x \tag{2.199}$$

The eigenstates associated to eigenvalues $\pm\Omega/2$ of $\hbar\Omega/2\sigma_x$ are

$$|+\rangle = \frac{|0\rangle + |1\rangle}{\sqrt{2}}$$
$$|-\rangle = \frac{|0\rangle - |1\rangle}{\sqrt{2}}$$

The Hamiltonian can be rewritten in the basis of $|\mp\rangle$. Under this basis change, the above operators can be replaced by

$$\sigma_z \to \sigma_x$$
$$\sigma_x \to \sigma_z$$

In this basis, the Hamiltonian becomes

$$\widetilde{\mathcal{H}} = \frac{1}{2}\hbar\Omega\sigma_z + \hbar\frac{\delta(t)}{2}\sigma_x \tag{2.200}$$

Using Fermi-Golden rule (see Eq. (2.130)), we get

$$\boxed{\Gamma_\varphi = \Gamma_{+-} = \frac{\pi}{2}\left(\frac{\partial\omega_{01}}{\partial\lambda}\right)^2 (S_\lambda\,(+\Omega))} \tag{2.201}$$

The equations of motion of the density operator in this new frame $\widetilde{\rho}$ should also include Lindblad jump operators expressed in the same frame. Under this transformation, the Lindblad jump operator becomes $\widetilde{L}_1 = \sqrt{\Gamma_1}\left(\sigma_z + i\sigma_y\right)/2$. Introducing this transformed operator into the equations of motion for σ^+operator (Eq. (2.218)), we get

$$\boxed{\Gamma_2 = \frac{3}{4}\Gamma_1 + \Gamma_\varphi} \tag{2.202}$$

This rate corresponds to the decay rate of the so-called Rabi oscillations.

2.5 Appendix

2.5.1 Master Equation Formalism

The quantum state of a qubit register is fragile and evolve in a non-unitary way, making it impossible to model its evolution using Schrodinger equation alone. The Master Equation formalism allows to treat the qubit register as an open system which interacts with its environment [33, 34].

2.5.1.1 Density Matrix Representation

The density matrix ρ for a system is a positive semi-definite Hermitian operator of trace one acting on the Hilbert space of the system. It is a generalization of the more usual state vectors or wavefunctions: while those can only represent pure states, density matrices can also represent mixed states, i.e. states where the physical system under study is entangled with its environment.

The general description of a density operator is

$$\rho = \sum_j p_j \left|\psi_j\right\rangle\left\langle\psi_j\right| \tag{2.203}$$

where $\left|\psi_j\right\rangle$ is a pure state of the system and p_j its probability. A density operator represents a pure state ($\rho = |\psi\rangle\langle\psi|$) if and only if $\mathrm{tr}(\rho^2) = 1$.

Interestingly, the expectation value of an operator O is given by

$$\boxed{\langle O(t)\rangle = \mathrm{Tr}\left[O\rho(t)\right]} \tag{2.204}$$

2.5.1.2 Density Matrix of a Qubit

For a single qubit, the density operator is a 2×2 matrix and can be written as

$$\rho = \frac{1}{2}\left(\mathbb{1} + \vec{P}.\vec{\sigma}\right) \tag{2.205}$$

where $\overrightarrow{\sigma} = (\sigma_x, \sigma_y, \sigma_z)$ represents a vector of Pauli matrices, and $\overrightarrow{P}$ represents a vector of the so-called Bloch sphere.

It is important to emphasize the difference between a probabilistic mixture of quantum states and their superposition. For instance, if the qubit is prepared as a statistical mixture of eigenstates $|0\rangle$ and $|1\rangle$ with equal probability, it can be described by the density matrix operator

$$\rho = \frac{1}{2}\begin{pmatrix} 1 & 0 \\ 0 & 1 \end{pmatrix} \tag{2.206}$$

On the other hand, a quantum superposition of these two states with equal probability amplitudes results in the pure state $|\psi\rangle = \frac{1}{\sqrt{2}}(|0\rangle + |1\rangle)$ and is associated with density matrix operator

$$\rho = \frac{1}{2}\begin{pmatrix} 1 & 1 \\ 1 & 1 \end{pmatrix} \tag{2.207}$$

In a general manner, the state of a qubit is a pure state if $\left|\overrightarrow{P}\right| = 1$ and is entangled with the environment if $\left|\overrightarrow{P}\right| < 1$.

2.5.1.3 Liouville-von Neumann Equation

The time evolution of the density operator is directly obtained from Schrodinger equation

$$\dot{\rho} = \sum_j p_j \left(|\partial_t \psi_j\rangle\langle\psi_j| + |\psi_j\rangle\langle\partial_t \psi_j|\right) = \frac{1}{i\hbar}\sum_j p_j \left(\mathcal{H}|\psi_j\rangle\langle\psi_j| - |\psi_j\rangle\langle\psi_j|\mathcal{H}\right)$$
$$= \frac{1}{i\hbar}\left[\mathcal{H}, \rho\right]$$

The evolution of the density operator according to Louville-von Neumann equation is unitary. However, a quantum system interacts with its environment and thus some unavoidable non-unitary evolution will happen.

2.5.1.4 Krauss Theorem

In general, any evolution of a quantum system can be described by a quantum map [33, 34] . Such quantum map is a linear super-operator that transforms the density operator ρ into a new operator $\mathcal{L}(\rho)$. To be valid, the quantum map must fulfill several conditions:

- **Linearity**—The super-operator must be linear $\mathcal{L}(\alpha\rho + \beta\rho') = \alpha\mathcal{L}(\rho) + \beta\mathcal{L}(\rho')$ with $\alpha + \beta = 1$.
- **Preservation of the trace**—The super-operator must conserve the trace of the density matrix $\mathrm{tr}(\mathscr{L}(\rho)) = 1$

- **Complete positivity**—$\mathcal{L}(\rho)$ must be positive semi-definite for any composite quantum system including the system and parts of its environment.

Under these conditions, the Krauss theorem states that any quantum map can be expressed as a sum of operators

$$\mathscr{L}(\rho) = \sum_{\mu=0}^{K-1} M_\mu \rho M_\mu^+ \tag{2.208}$$

where one can choose $K - 1 < d^2$, d being the dimension of the Hilbert space of the system and K is the Krauss number. In order to conserve the trace, it is straightforward to show that the Krauss operators M_μ must satisfy the normalization condition

$$\sum_{\mu=0}^{K-1} M_\mu^+ M_\mu = \mathbb{1} \tag{2.209}$$

2.5.1.5 Lindblad Equation

Assuming the system is Markovian (no memory), we define the derivative of the density operator as

$$\dot{\rho} = \frac{\mathscr{L}_\tau(\rho) - \rho}{\tau} \tag{2.210}$$

In order to be defined for infinitesimal τ, one of the Krauss operators M_0 should satisfy the condition $\lim_{\tau \to 0} M_0 = \mathbb{1}$. At first order in τ, we can thus write it as

$$M_0 = \mathbb{1} - \boldsymbol{i} L_0 \tau \tag{2.211}$$

We write the operator L_0 as a sum of hermitian and antihermitian operators $L_0 = \frac{1}{2}\left(L_0 + L_0^+\right) + \frac{1}{2}\left(L_0 - L_0^+\right)$ and introduce $H = \frac{\hbar}{2}\left(L_0 + L_0^+\right)$ and $J = \frac{\boldsymbol{i}}{2}\left(L_0 - L_0^+\right)$. Up to first order in τ, we have

$$M_0 \rho M_0^+ = \rho - \boldsymbol{i}\tau/\hbar\,[H, \rho] - \tau\,(J\rho + \rho J) \tag{2.212}$$

All other Krauss operators ($\mu \neq 0$) will contribute at first order only and thus can be written as

$$M_\mu = \sqrt{\tau} L_\mu \tag{2.213}$$

Using the normalization condition, we get

$$\sum_{\mu=0}^{K-1} M_\mu^+ M_\mu = \mathbb{1} - 2J\tau + \tau \sum_{\mu \neq 0} L_\mu^+ L_\mu = \mathbb{1} \tag{2.214}$$

we can thus express J as a function of L_μ as

$$J = \frac{1}{2}\sum_{\mu\neq 0} L_\mu^+ L_\mu \tag{2.215}$$

Reorganizing the terms of the equation, we get the Lindblad equation

$$\boxed{\frac{d}{dt}\rho = -\frac{i}{\hbar}[H,\rho] + \sum_{\mu\neq 0} L_\mu \rho L_\mu^\dagger - \tfrac{1}{2}\left(L_\mu^\dagger L_\mu \rho + \rho L_\mu^\dagger L_\mu\right)} \tag{2.216}$$

2.5.1.6 Equations of Motion

For a system described by the Lindblad master-equation, the time evolution of an arbitrary operator $O(t)$ is given by

$$\frac{d}{dt}\langle O(t)\rangle = \frac{d}{dt}\mathrm{Tr}\left[O\rho(t)\right] = \mathrm{Tr}\left[O\frac{d}{dt}\rho(t)\right] \tag{2.217}$$

Using Eq. (2.216), and noting that

$$\begin{aligned}
\mathrm{Tr}\left[O\left[H,\rho\right]\right] &= \mathrm{Tr}\left[\left[O,H\right]\rho\right] = \langle[O(t),H]\rangle \\
\mathrm{Tr}\left[OL_\mu\rho L_\mu^\dagger\right] &= \mathrm{Tr}\left[L_\mu^\dagger O L_\mu \rho\right] = \left\langle L_\mu^\dagger O(t) L_\mu\right\rangle \\
\mathrm{Tr}\left[O\rho L_\mu^\dagger L_\mu\right] &= \mathrm{Tr}\left[L_\mu^\dagger L_\mu O\rho\right] = \left\langle L_\mu^\dagger L_\mu O(t)\right\rangle \\
\mathrm{Tr}\left[OL_\mu^\dagger L_\mu\rho\right] &= \left\langle O(t) L_\mu^\dagger L_\mu\right\rangle
\end{aligned}$$

We get

$$\boxed{\frac{d}{dt}\langle O(t)\rangle = \frac{i}{\hbar}\langle[H,O(t)]\rangle + \sum_{\mu\neq 0}\left(\left\langle L_\mu^\dagger O(t) L_\mu\right\rangle - \frac{1}{2}\left\langle L_\mu^\dagger L_\mu O(t)\right\rangle - \frac{1}{2}\left\langle O(t) L_\mu^\dagger L_\mu\right\rangle\right)} \tag{2.218}$$

2.5.1.7 Some Simple Examples

As a matter of illustration, we will consider in the following two simple examples.

- **Cavity with damping**

In this first example, we consider the equation of motion of an harmonic oscillator driven by a classical field assuming an Hamiltonian $\mathcal{H} = \hbar\omega_r a^+ a + \hbar\varepsilon(a + a^+)$

in presence of a Lindblad jump operator $L = \sqrt{\kappa}a$, where ω_r is the resonance frequency of the resonator and ε the strength of the field. Using Eq. (2.218), we get

$$\frac{da}{dt} = -\boldsymbol{i}\omega_r a - \boldsymbol{i}\varepsilon - \frac{\kappa}{2}a \tag{2.219}$$

from which we obtain that

$$a[\omega] = \frac{-\boldsymbol{i}\varepsilon[\omega]}{\boldsymbol{i}(\omega_r - \omega) + \kappa/2} \tag{2.220}$$

- **Qubit evolution under classical drive**

In this second example, we consider the equations of motion of a qubit driven by a classical field assuming an Hamiltonian $\mathcal{H} = \frac{1}{2}\hbar\delta\sigma_z + \frac{1}{2}\hbar\Omega\sigma_x$ in presence of Lindblad jump operators $L_1 = \sqrt{\Gamma_1}\sigma^-$ and $L_\varphi = \sqrt{\frac{\Gamma_\varphi}{2}}\sigma_z$ where $\delta = \omega_{01} - \omega_P$ is the detuning between the pump and the resonance frequency of the qubit and Ω is the Rabi frequency. Using Eq. (2.218), we get

$$\begin{aligned}
\frac{d\sigma_x}{dt} &= -\delta\sigma_y - \left(\frac{\Gamma_1}{2} + \Gamma_\varphi\right)\sigma_x \\
\frac{d\sigma_y}{dt} &= \delta\sigma_x - \Omega\sigma_z - \left(\frac{\Gamma_1}{2} + \Gamma_\varphi\right)\sigma_y \\
\frac{d\sigma_z}{dt} &= \Omega\sigma_y - \Gamma_1(\sigma_z + \mathbb{1}) \\
\frac{d\mathbb{1}}{dt} &= 0
\end{aligned}$$

This system of equations can be written in a matrix for with $\overrightarrow{O} = \left(\sigma_x(t), \sigma_y(t), \sigma_z(t)\ \mathbb{1}\right)^T$ as $\frac{d}{dt}\overrightarrow{O}(t) = G\overrightarrow{O}(t)$ with

$$G = \begin{pmatrix} -\left(\frac{\Gamma_1}{2} + \Gamma_\varphi\right) & -\delta & 0 & 0 \\ \delta & -\left(\frac{\Gamma_1}{2} + \Gamma_\varphi\right) & -\Omega & 0 \\ 0 & \Omega & -\Gamma_1 & -\Gamma_1 \\ 0 & 0 & 0 & 0 \end{pmatrix} \tag{2.221}$$

The steady-state expectation values are obtained by the null eigenstate of G, defined by $G\langle \boldsymbol{O}\rangle = 0$, leading to

$$\langle\sigma_x\rangle_\infty = \frac{\delta\Omega T_2^2}{1 + \delta^2 T_2^2 + \Omega^2 T_1 T_2} w_0 \tag{2.222}$$

$$\langle \sigma_y \rangle_\infty = \frac{\Omega T_2}{1 + \delta^2 T_2^2 + \Omega^2 T_1 T_2} w_0 \tag{2.223}$$

$$\langle \sigma_z \rangle_\infty = \frac{1 + \delta^2 T_2^2}{1 + \delta^2 T_2^2 + \Omega^2 T_1 T_2} w_0 \tag{2.224}$$

where $\frac{1}{T_2} = \frac{\Gamma_1}{2} + \Gamma_\varphi$ and w_0 is the expectation value of σ_z when the system is not driven ($\Omega = 0$).

2.5.1.8 Quantum Regression Theorem

As shown in the example herein above, it is often possible to write an equation of motion for an operator $A(t)$ as a linear combination of a set of system's operators B_j, namely

$$\frac{d}{dt}\langle A(t) \rangle = \sum_j G_j \langle B_j(t) \rangle \tag{2.225}$$

Using Lindblad master-equation $\frac{d\rho}{dt} = \mathscr{L}\rho$, we can thus write

$$\mathrm{Tr}\left[A \mathscr{L} \rho\right] = \mathrm{Tr}\left[\sum_j G_j B_j \rho\right] \tag{2.226}$$

This equation being satisfied for any $\rho(t)$, we obtain that

$$A\mathcal{L} = \sum_j G_j B_j \tag{2.227}$$

This result allows us to compute the time derivative

$$\frac{d}{d\tau}\langle A(t+\tau) O(t) \rangle = \frac{d}{d\tau} \mathrm{Tr}\left[A e^{\mathcal{L}\tau} O \rho(t)\right] \tag{2.228}$$

$$= \mathrm{Tr}\left[A \mathcal{L} e^{\mathcal{L}\tau} O \rho(t)\right]. \tag{2.229}$$

Using Eq. (2.227) we obtain

$$\frac{d}{d\tau}\langle A(t+\tau) O(t) \rangle = \mathrm{Tr}\left[\sum_j G_j B_j e^{\mathcal{L}\tau} O \rho(t)\right] \tag{2.230}$$

$$= \sum_j G_j \mathrm{Tr}\left[B_j e^{\mathcal{L}\tau} O\rho(t)\right] \tag{2.231}$$

$$= \sum_j G_j \langle B_j(t+\tau) O(t)\rangle \tag{2.232}$$

Equation (2.232) is the quantum regression theorem [32].

2.5.2 Schrieffer Wolff Transformation

2.5.2.1 Unitary Transformation

Let's consider a unitary transformation $U(t)$ acting on the Hilbert space $\mathcal{E}_H$ and characterized by the relation $U^+U = \mathbb{1}$. Under this transformation, the state of the system $|\Psi\rangle$ becomes $\left|\widetilde{\Psi}\right\rangle = U(t)|\Psi\rangle$. Writing the Schrodinger equation for $\left|\widetilde{\Psi}\right\rangle$ gives

$$\begin{aligned} i\hbar\partial_t \left|\widetilde{\Psi}\right\rangle &= i\hbar\partial_t \left(U(t)|\Psi\rangle\right) = i\hbar\partial_t U(t)|\Psi\rangle + i\hbar U(t)\partial_t|\Psi\rangle \\ &= i\hbar\partial_t U(t)U^+(t)\left|\widetilde{\Psi}\right\rangle + U(t)H|\Psi\rangle \\ &= \left(i\hbar\partial_t U(t)U^+(t) + U(t)HU^+(t)\right)\left|\widetilde{\Psi}\right\rangle \end{aligned}$$

Thus, under this unitary transformation the Hamiltonian becomes

$$\boxed{\widetilde{H} = U(t)HU^+(t) + i\hbar\dot{U}(t)U^+(t)} \tag{2.233}$$

In particular, if the unitary transformation does not depend on time, $\widetilde{H} = UHU^+$. If the transformation is time dependent, a new term will be added in the Hamiltonian. This term is the quantum equivalent of fictitious forces that appear in a non-inertial frame of reference in classical physics.

2.5.2.2 Baker Campbell Hausdorff Formula

For two operators A and B, we consider the expression $\widetilde{B}(\lambda) = e^{\lambda A}Be^{-\lambda A}$ where $\lambda \in \mathbb{C}$. The Baker Campbell Hausdorff formula states that it is possible to express $\widetilde{B}(\lambda)$ as a formal series of operators A and B and iterated commutators thereof, namely

$$\begin{aligned} \widetilde{B}(\lambda) = e^{\lambda A}Be^{-\lambda A} &= B + \lambda[A,B] + \frac{\lambda^2}{2}[A,[A,B]] \\ &+ \ldots + \frac{\lambda^n}{n!}[A,[A,\ldots\ [A,B]]]]]_n \end{aligned} \tag{2.234}$$

The demonstration of this formula is extremely simple. For $\lambda = 0$, the formula is true. Moreover, it is straightforward to show that the two sides of the equality are solutions of the same linear first order differential equation

$$\frac{\partial \widetilde{B}(\lambda)}{\partial \lambda} = \left[A, \widetilde{B}(\lambda)\right] \tag{2.235}$$

Thus, according to the Cauchy Lipschitz theorem, the two sides of the equation must be identical.

2.5.2.3 Schrieffer Wolff Transformation

In quantum mechanics, the Schrieffer–Wolff transformation is a unitary transformation used to simplify the Hamiltonian of a system $H = H_0 + V$ to second order in the interaction V. Under a unitary transformation, the Hamiltonian of the system becomes

$$\widetilde{H} = e^S H e^{-S} \tag{2.236}$$

where S is an anti-hermitian operator. Using Baker Campbell Hausdorff formula

$$\begin{aligned}\widetilde{H} = H_0 + V + [S, H_0 + V] + \frac{1}{2}[S, [S, H_0 + V]] \\ + \ldots + \frac{1}{n!}[S, [S, \ldots\ [S, H_0 + V]]]]]_n\end{aligned} \tag{2.237}$$

If one chooses properly S such that

$$[S, H_0] = -V \tag{2.238}$$

$$\widetilde{H} = H_0 + V - V + [S, V] - \frac{1}{2}[S, V] + \frac{1}{2}[S, [S, V]] + \ldots$$

Thus, the transformed Hamiltonian can be written up to second order in V as

$$\boxed{\widetilde{H} = H_0 + \frac{1}{2}[S, V] + O(V^3)} \tag{2.239}$$

2.5.2.4 A Simple Application of Schrieffer Wolff Transformation

As an illustration, we consider we consider the Hamiltonian of a spin coupled non-resonantly to a resonator (assuming for simplicity rotating wave approximation). The Hamiltonian of the system can be written as

$$\mathcal{H} = \hbar\omega_r a^+ a + \frac{1}{2}\hbar\omega_{01}\sigma_z + \hbar g\left(\sigma^+ a + \sigma^- a^+\right) \tag{2.240}$$

We consider the coupling term $V = \hbar g\left(\sigma^+ a + \sigma^- a^+\right)$ as a small perturbation and introduce the operator $S = \frac{g}{\omega_{01}-\omega_r}\left(\sigma^+ a - \sigma^- a^+\right)$. It is easy to check that S is anti-hermitian $\left(S = -S^+\right)$ and that

$$\frac{g}{\omega_{01}-\omega_r}\left[\left(\sigma^+ a - \sigma^- a^+\right), \omega_r a^+ a + \frac{1}{2}\omega_{01}\sigma_z\right] = -g\left(\sigma^+ a + \sigma^- a^+\right) = -V \tag{2.241}$$

The commutator $[S, V]$ can be calculated straightforwardly

$$[S, V] = \frac{\hbar g^2}{\omega_{01}-\omega_r}\left[\sigma^+ a - \sigma^- a^+, \sigma^+ a + \sigma^- a^+\right] = \frac{2\hbar g^2}{\omega_{01}-\omega_r}\left[\sigma^+ a, \sigma^- a^+\right] \tag{2.242}$$

Thus, the transformed Hamiltonian can be written as

$$\boxed{\widetilde{H} \simeq \hbar\omega_r a^+ a + \frac{1}{2}\hbar\omega_{01}\sigma_z + \frac{\hbar g^2}{(\omega_{01}-\omega_r)}\sigma_z\left(a^+ a + \frac{1}{2}\right)} \tag{2.243}$$

This Hamiltonian exhibits the so-called dispersive shift of the resonator. The resonance frequency of the resonator is slightly shifted from its bare resonance due to the presence of the spin. The sign of this shift depends on the state of the spin and thus is used frequently in circuit QED for reading out a qubit state. Inversely, the number of photons in the resonator will give rise to a shift in the transition frequency of the spin (Lamb shift). This reverse effect is in general detrimental for the spin coherence. Shot noise of photons in the resonator (photon noise) will give rise to noise in the resonance frequency of the spin which will lead to loss of coherence.

Acknowledgments The material of this book chapter is based on lectures on superconducting quantum circuits given at Bar Ilan University (Ramat Gan, Israel) from 2016 to 2022, at GradNet Quantum Computing workshop (April 2021) and at the International Training course in the Physics of Strongly Correlated Systems (October 2021). I wish to thank my wife, Myriam, for her constant encouragement and support over the years, inspiring me to write these notes and bringing this book chapter to life. We are indebted to all the colleagues, students, postdocs and visitors who have worked with us over the years. In particular, I wish to thank D. Esteve, P. Bertet, D. Vion, M. Devoret, E. Dalla Torre, E. Ginossar, G. Catelani, T. Chang, I. Holzman, P. Brookes, I. Shani and T. Cohen for numerous discussions and collaborative works that have led to this manuscript.

References

1. M. Tinkham, *Introduction to Superconductivity*, 2nd edn. (Dover Publications, Mineola, 2004). http://www.worldcat.org/isbn/0486435032 64, 85
2. J. Millman, Proc. IRE **28**(9), 413 (1940). https://doi.org/10.1109/JRPROC.1940.225885 66, 71
3. D.M. Pozar, *Microwave Engineering*, 4th edn. (Wiley, New Delhi, 2012). Includes index 67

4. A. Caldeira, A. Leggett, Ann. Phys. **149**(2), 374 (1983). https://doi.org/10.1016/0003-4916(83)90202-6 70
5. B. Yurke, J.S. Denker, Phys. Rev. A **29**, 1419 (1984). https://doi.org/10.1103/PhysRevA.29.1419 70
6. V. Bouchiat, D. Vion, P. Joyez, D. Esteve, M.H. Devoret, Phys. Scripta **1998**(T76), 165 (1998). https://doi.org/10.1238/Physica.Topical.076a00165 82
7. Y. Nakamura, Y.A. Pashkin, J.S. Tsai, Nature **398**(6730), 786 (1999). https://doi.org/10.1038/19718 82
8. J. Koch, T.M. Yu, J. Gambetta, A.A. Houck, D.I. Schuster, J. Majer, A. Blais, M.H. Devoret, S.M. Girvin, R.J. Schoelkopf, Phys. Rev. A **76**, 042319 (2007). https://doi.org/10.1103/PhysRevA.76.042319 86
9. H. Paik, D.I. Schuster, L.S. Bishop, G. Kirchmair, G. Catelani, A.P. Sears, B.R. Johnson, M.J. Reagor, L. Frunzio, L.I. Glazman, S.M. Girvin, M.H. Devoret, R.J. Schoelkopf, Phys. Rev. Lett. **107**, 240501 (2011). https://doi.org/10.1103/PhysRevLett.107.240501 87, 94, 95, 111
10. R. Barends, J. Kelly, A. Megrant, D. Sank, E. Jeffrey, Y. Chen, Y. Yin, B. Chiaro, J. Mutus, C. Neill, P. O'Malley, P. Roushan, J. Wenner, T.C. White, A.N. Cleland, J.M. Martinis, Phys. Rev. Lett. **111**, 080502 (2013). https://doi.org/10.1103/PhysRevLett.111.080502 87, 111
11. A.P.M. Place, L.V.H. Rodgers, P. Mundada, B.M. Smitham, M. Fitzpatrick, Z. Leng, A. Premkumar, J. Bryon, A. Vrajitoarea, S. Sussman, G. Cheng, T. Madhavan, H.K. Babla, X.H. Le, Y. Gang, B. Jäck, A. Gyenis, N. Yao, R.J. Cava, N.P. de Leon, A.A. Houck, Nat. Commun. **12**(1) (2021). https://doi.org/10.1038/s41467-021-22030-5 87, 111
12. Y. Sung, L. Ding, J. Braumüller, A. Vepsäläinen, B. Kannan, M. Kjaergaard, A. Greene, G.O. Samach, C. McNally, D. Kim, A. Melville, B.M. Niedzielski, M.E. Schwartz, J.L. Yoder, T.P. Orlando, S. Gustavsson, W.D. Oliver, Phys. Rev. X **11**, 021058 (2021). https://doi.org/10.1103/PhysRevX.11.021058 87, 102
13. J.E. Mooij, T.P. Orlando, L. Levitov, L. Tian, C.H. van der Wal, S. Lloyd, Science **285**(5430), 1036 (1999). https://doi.org/10.1126/science.285.5430.1036 87
14. I. Chiorescu, Y. Nakamura, C.J.P.M. Harmans, J.E. Mooij, Science **299**(5614), 1869 (2003). https://doi.org/10.1126/science.1081045
15. F. Yoshihara, K. Harrabi, A.O. Niskanen, Y. Nakamura, J.S. Tsai, Phys. Rev. Lett. **97**, 167001 (2006). https://doi.org/10.1103/PhysRevLett.97.167001
16. J. Bylander, S. Gustavsson, F. Yan, F. Yoshihara, K. Harrabi, G. Fitch, D.G. Cory, Y. Nakamura, J.S. Tsai, W.D. Oliver, Nat. Phys. **7**(7), 565 (2011). https://doi.org/10.1038/nphys1994 118
17. M. Stern, G. Catelani, Y. Kubo, C. Grezes, A. Bienfait, D. Vion, D. Esteve, P. Bertet, Phys. Rev. Lett. **113**, 123601 (2014). https://doi.org/10.1103/PhysRevLett.113.123601 87, 111
18. T. Chang, I. Holzman, T. Cohen, B.C. Johnson, D.N. Jamieson, M. Stern, Phys. Rev. Appl. **18**, 064062 (2022). https://doi.org/10.1103/PhysRevApplied.18.064062 93, 111
19. F.G. Paauw, A. Fedorov, C.J.P.M. Harmans, J.E. Mooij, Phys. Rev. Lett. **102**, 090501 (2009). https://doi.org/10.1103/PhysRevLett.102.090501 93
20. T. Chang, T. Cohen, I. Holzman, G. Catelani, M. Stern, Phys. Rev. Appl. **19**, 024066 (2023). https://doi.org/10.1103/PhysRevApplied.19.024066 93
21. V.E. Manucharyan, J. Koch, L.I. Glazman, M.H. Devoret, Science **326**(5949), 113 (2009). https://doi.org/10.1126/science.1175552 94
22. I.M. Pop, K. Geerlings, G. Catelani, R.J. Schoelkopf, L.I. Glazman, M.H. Devoret, Nature **508**(7496), 369 (2014). https://doi.org/10.1038/nature13017 94
23. L.B. Nguyen, Y.H. Lin, A. Somoroff, R. Mencia, N. Grabon, V.E. Manucharyan, Phys. Rev. X **9**, 041041 (2019). https://doi.org/10.1103/PhysRevX.9.041041 94
24. F. Yan, S. Gustavsson, A. Kamal, J. Birenbaum, A.P. Sears, D. Hover, T.J. Gudmundsen, D. Rosenberg, G. Samach, S. Weber, J.L. Yoder, T.P. Orlando, J. Clarke, A.J. Kerman, W.D. Oliver, Nat. Commun. **7**(1), 12964 (2016). https://doi.org/10.1038/ncomms12964 94
25. L.V. Abdurakhimov, I. Mahboob, H. Toida, K. Kakuyanagi, S. Saito, Appl. Phys. Lett. **115**(26), 262601 (2019). https://doi.org/10.1063/1.5136262 94, 111
26. A. Blais, A.M. van den Brink, A.M. Zagoskin, Phys. Rev. Lett. **90**, 127901 (2003). https://doi.org/10.1103/PhysRevLett.90.127901 102

27. J. Majer, J.M. Chow, J.M. Gambetta, J. Koch, B.R. Johnson, J.A. Schreier, L. Frunzio, D.I. Schuster, A.A. Houck, A. Wallraff, A. Blais, M.H. Devoret, S.M. Girvin, R.J. Schoelkopf, Nature **449**(7161), 443 (2007). https://doi.org/10.1038/nature06184 102
28. C. Rigetti, A. Blais, M. Devoret, Phys. Rev. Lett. **94**, 240502 (2005). https://doi.org/10.1103/PhysRevLett.94.240502 105
29. C. Rigetti, M. Devoret, Phys. Rev. B **81**, 134507 (2010). https://doi.org/10.1103/PhysRevB.81.134507 105
30. S. Kirchhoff, T. Keßler, P.J. Liebermann, E. Assémat, S. Machnes, F. Motzoi, F.K. Wilhelm, Phys. Rev. A **97**, 042348 (2018). https://doi.org/10.1103/PhysRevA.97.042348 105
31. G. Ithier, E. Collin, P. Joyez, P.J. Meeson, D. Vion, D. Esteve, F. Chiarello, A. Shnirman, Y. Makhlin, J. Schriefl, G. Schön, Phys. Rev. B **72**, 134519 (2005). https://doi.org/10.1103/PhysRevB.72.134519 115, 116
32. I. Shani, E.G. Dalla Torre, M. Stern, Phys. Rev. A **105**, 022617 (2022). https://doi.org/10.1103/PhysRevA.105.022617 118, 128
33. S. Haroche, J.M. Raimond, *Exploring the Quantum* (Oxford University Press, Oxford, 2006). https://doi.org/10.1093/acprof:oso/9780198509141.001.0001 122, 123
34. H.M. Wiseman, G.J. Milburn, *Quantum Measurement and Control* (Cambridge University Press, Cambridge, 2009) 122, 123

3 Subgap States in Semiconductor-Superconductor Devices for Quantum Technologies: Andreev Qubits and Minimal Majorana Chains

Rubén Seoane Souto and Ramón Aguado

Abstract

In recent years, experimental advances have made it possible to achieve an unprecedented degree of control over the properties of subgap bound states in hybrid nanoscale superconducting structures. This research has been driven by the promise of engineering subgap states for quantum applications, including Majorana zero modes predicted to appear at the interface of superconductor and other materials, like topological insulators or semiconductors. In this chapter, we revise the status of the field towards the engineering of quantum devices in controllable semiconductor-superconductor heterostructures. We begin the chapter with a brief introduction about subgap states, focusing on their mathematical formulation. After introducing topological superconductivity using the Kitaev model, we discuss the advances in the search for Majorana states over the last few years, highlighting the difficulties of unambiguously distinguish these states from nontopological subgap states. In recent years, the precise engineering of bound states by a bottom-up approach using quantum dots has led to unprecedented experimental advances, including experimental demonstrations of Andreev qubits based on a quantum dot Josephson junctions and a minimal Kitaev chains based on two quantum dots coherently coupled by the bound states of an intermediate superconducting segment. These experimental advances have revitalized the field and helped to understand that, far from being a disadvantage, the presence of subgap bound states can be exploited for new qubit designs and quantum coherence experiments, including Majorana-based qubits.

R. Seoane Souto · R. Aguado (✉)
Instituto de Ciencia de Materiales de Madrid (ICMM), Consejo Superior de Investigaciones Científicas (CSIC), Madrid, Spain
e-mail: ruben.seoane@csic.es; ramon.aguado@csic.es

R. Aguado et al. (eds.), *New Trends and Platforms for Quantum Technologies*,
Lecture Notes in Physics 1025, https://doi.org/10.1007/978-3-031-55657-9_3